This article has been accepted for publication in a future issue of this journal, but has not been fully edited. Content may change prior to final publication. Citation information: DOI 10.1109/JSAC.2016.2551619, IEEE Journal on Selected Areas in Communications

Adaptively Directional Wireless Power Transfer for Large-scale Sensor Networks

Zhe Wang, *Member, IEEE*, Lingjie Duan, *Member, IEEE*, and Rui Zhang, *Senior Member, IEEE*

***Abstract*—Wireless power transfer (WPT) prolongs the lifetime of wireless sensor network by providing sustainable power supply to the distributed sensor nodes (SNs) via electromagnetic waves. To improve the energy transfer efficiency in a large WPT system, this paper proposes an adaptively directional WPT (AD-WPT) scheme, where the power beacons (PBs) adapt the energy beamforming strategy to SNs' locations by concentrating the transmit power on the nearby SNs within the efficient charging radius. With the aid of stochastic geometry, we derive the expressions of the distribution metrics of the aggregate received power at a typical SN. To design the charging radius for the optimal AD-WPT operation, we exploit the tradeoff between the power intensity of the energy beams and the number of SNs to be charged. Depending on different SN task requirements, the optimal AD-WPT can maximize the average received power or the active probability of the SNs, respectively. It is shown that both the maximum average received power and the maximum sensor active probability increase with the increased deployment density and transmit power of the PBs, and decrease with the increased density of the SNs and the energy beamwidth. Finally, we show that the optimal AD-WPT can significantly improve the energy transfer efficiency compared with the traditional omnidirectional WPT.**

***Index Terms*—Wireless power transfer, adaptively directional transmission, energy beamforming, average power maximization, active probability maximization, sensor network, stochastic geometry.**

I. Introduction

Wireless sensor networks (WSNs) consist of small-size, low-power and distributed sensor nodes (SNs) to monitor physical or environmental conditions [1]. WSNs are often required to operate for long periods of time, but the network lifetime is constrained by the limited battery capacity and costly battery replacement at SNs. To extend the network lifetime, it is desirable to recharge the SNs in an undisruptive and energy efficient way.

RF-enabled wireless power transfer (WPT) [2], [3] provides a controllable and sustainable power supply to sensor network by charging SNs via electromagnetic (EM) waves [4]–[6]. There are mainly two types of WPT: omnidirectional WPT and directional WPT. For omnidirectional WPT, the energy transmitter or so-called power beacon (PB) broadcasts the EM waves equally in all directions regardless of the locations of the energy receivers. According to the law of conservation of energy, the energy radiated in the directions of energy receivers accounts for only a small fraction of the total radiated power. Since the EM waves fade rapidly over distance, it may require excessively high transmit power to charge an energy receiver via omnidirectional WPT, which may not be energy efficient. In contrast, for directional WPT with antenna arrays, the PB concentrates the radiated energy in the directions of the energy receivers, i.e., via energy beamforming, which enhances the power intensity in the intended directions. The energy transfer efficiency is thus improved with the consequent reduction of transmit power to reach the target received power.

Most of the literature on directional WPT (see [2] and references therein) has focused on point-to-point and point-to-multipoint transmissions. For a large-scale WSN, the SNs are often in large quantities and are usually distributed with random locations. There are two main challenges in the design of directional WPT for a large-scale network. On the *PB-side*, it is challenging to adapt the energy beamforming strategy to the random locations of the SNs, e.g., to decide which SNs to serve, how many beams to generate and the beamwidth of each beam, etc. On the *SN-side*, it is difficult to analyze the aggregate received power from a large number of PBs in the network, where the radiation directions and energy intensity may vary for each PB.

In this paper, we aim at tackling the above two challenges. The paper's structure and main contributions are given as follows.

- *Energy-efficient AD-WPT scheme to power a large-scale sensor network*: To address the PB-side challenge, we propose an adaptively directional WPT (AD-WPT) scheme in a large-scale sensor network in Section II, where the energy beamforming strategy of the PBs is adaptive to the nearby SN locations that are within the energy-efficient charging radius. To deal with the tradeoff between the power intensity of the energy beams and the number of SNs served by each PB, we design the charging radius to achieve optimal AD-WPT for different performance targets, i.e., average power maximization or active probability maximization. The sensor active probability is defined as the probability that the received power at the SN exceeds a target received power threshold.
- *Analysis of harvested power using stochastic geometry*: To address the SN-side challenge, in Section III, we successfully derive the distribution metrics, e.g., Laplace transform, mean, variance, and complementary cumulative distribution function (CCDF) of the aggregate re-

Part of this work was presented at the IEEE Global Communications Conference (GLOBECOM 2015), San Diego, CA, USA, Dec. 6-10, 2015. This work is supported by the SUTD-ZJU Joint Collaboration Grant (Project Number: SUTD-ZJU/RES/03/2014).

Z. Wang and L. Duan are with Pillar of Engineering Systems and Design, Singapore University of Technology and Design, Singapore (e-mail: wangzhe.annie@gmail.com; lingjie_duan@sutd.edu.sg).

R. Zhang is with the Department of Electrical and Computer Engineering, National University of Singapore, Singapore (e-mail: elezhang@nus.edu.sg). He is also with the Institute for Infocomm Research, A*STAR, Singapore.

This article has been accepted for publication in a future issue of this journal, but has not been fully edited. Content may change prior to final publication. Citation information: DOI 10.1109/JSAC.2016.2551619, IEEE Journal on Selected Areas in Communications

ceived power at a typical SN from the large-scale PB network using the tools of stochastic geometry [7]–[10].

- *Optimal AD-WPT for average power maximization*: In flexible-task WSN, the SNs operate in a cooperative manner on power adaptive sensing tasks. To achieve the optimal AD-WPT in this case, we design the optimal charging radius to maximize the average received power of the SNs in Section IV. We show that the maximum average received power increases with the increased PB power and density, while it decreases with the increased energy beamwidth and SN density. In addition, the optimal AD-WPT greatly improves the average received power compared with omnidirectional WPT, especially when PB power/density is high.
- *Optimal AD-WPT for active probability maximization*: In equal-task WSN, the SNs operate in an independent manner on equal amounts of sensing tasks. An SN is active if its received power is beyond a given power threshold. To achieve the optimal AD-WPT in this case, we design the optimal charging radius to maximize the active probability of the SNs in Section V. It shows that the optimal AD-WPT can enhance the sensor active probability compared with omnidirectional WPT, especially when the PB power/density is not high.

In Section VI, the numerical results are shown and discussed. Finally, conclusions are drawn in Section VII.

A. Related Literature

Omnidirectional WPT has been studied recently in [11]–[19]. In [11], a point-to-point omnidirectional WPT is investigated, where the receiver utilizes part of the harvested energy for decoding the information in the received signal. In [12], the downlink energy transfer in a broadcast network is studied for throughput maximization. In [13], a stochastic geometry based model is considered for a cognitive radio network, where the secondary transmitters harvest RF energy from the nearby primary transmitters. [14] investigates the downlink energy transfer in a large-scale wireless network by considering finite and infinite battery capacity. In [15]–[19], cooperative relay is explored in wireless energy and information transfer system, where relay receives energy/information signal from source and forwards to destination. Directional WPT has been addressed in [20]–[23]. In [20], energy beamforming is studied in a broadcast network where the transmitter steers the energy beams towards the receivers to maximize their received power. In [21] and [22], energy beamforming is designed in a MIMO broadcast network jointly with information beamforming, where the transmitter adjusts the beam weights to maximize the received power and information rates at different receivers. In [23], each mobile node in a cellular network is charged by its nearest PB via energy beamforming. For the simplicity of analysis, only the received energy from the nearest PB is considered and that from all other PBs is omitted in [23]. With energy collaboration and load sharing among base stations, [24] and [25] study the energy cost saving and power consumption reduction in cellular networks, respectively.

To the best of our knowledge, this paper is the first study of directional WPT by using adaptive energy beamforming for a large-scale network and the resulting aggregate received power from all PBs with AD-WPT is rigorously characterized. With the proposed AD-WPT scheme, the energy transfer efficiency in the large-scale network can be greatly enhanced compared with the traditional omnidirectional WPT.

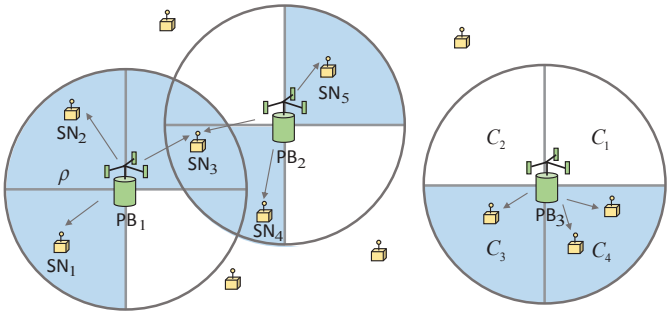

Fig. 1. System model of AD-WPT (illustrative example of $N = 4$). The circular areas with radius ρ are the charging regions of the PBs. The shaded sectors in the charging regions are the active sectors of the PBs.

II. System Model

We consider a wireless charging network as shown in Fig. 1, where a PB network wirelessly charges an SN network via energy beamforming. Each PB radiates EM waves with wavelength ν using transmit power P_p. The PBs and SNs follow two independent homogeneous Poisson Point Processes (PPPs) $\Phi_p = \{X_i\}$ and $\Phi_s = \{Y_j\}$ with density λ_p and λ_s, respectively, where X_i and Y_j represent the coordinates of the PBs and SNs in $\mathbb{R}^2$ plane.

In the following, we first propose a power transfer scheme with adaptive energy beamforming, and then discuss the radiated power intensity at the PBs and the aggregate received power at the typical SN from all PBs in the network. The key notations and their physical meanings are listed in Table I.

A. AD-WPT Scheme

Due to the significant attenuation of the radio power over the distance, it is more energy efficient for the PBs to focus the energy to charge the nearby SNs. With antenna arrays, a PB is able to form an energy beam in a certain direction or generate multiple beams simultaneously towards different directions [26]. In this subsection, we propose an AD-WPT scheme where the PBs adapt the beamforming strategy to the random locations of the SNs.

To decide which SNs to charge, we define *charging region* as a circular region centered at each PB with *charging radius* ρ, as shown in Fig. 1. We use the same charging radius for all PBs for the ease of implementation and analysis. Each charging region is divided into N equal sectors $C_1, \cdots, C_N$.[1] We consider that a PB is aware of the existence of the SNs inside each of its sectors, e.g., via the SN feedback over control channels. A sector is considered to be active if at least one

[1]The specific facing direction of each sector may change some SNs' received power in particular locations, but does not influence the analysis of a typical SN's total received power by averaging over all possible locations in the whole network.

This article has been accepted for publication in a future issue of this journal, but has not been fully edited. Content may change prior to final publication. Citation information: DOI 10.1109/JSAC.2016.2551619, IEEE Journal on Selected Areas in Communications

TABLE I
NOTATIONS AND PHYSICAL MEANINGS

Notation	Description	Notation	Description
λ_p	node density of PB network	λ_s	node density of SN network
Φ_p	PPP of density λ_p for PBs	Φ_s	PPP of density λ_s for SNs
ρ	charging radius	α	path loss exponent
$b(o,\rho)$	disk of radius ρ centered at the origin	ν	wavelength
X_i	coordinates of PBs	Y_j	coordinates of SNs
N	number of sectors per PB	M	number of active sectors of a PB
G_M	antenna gain of PB with M active sectors	p	probability that no SN is inside a sector
$\theta_{M,n}$	conditional event that SN_0 receives power from PB with antenna gain G_M given it is a near PB	$\theta_{M,f}$	conditional event that SN_0 receives power from PB with antenna gain G_M given it is a far PB
$\beta_{M,n}$	conditional probability that SN_0 receives power from PB with antenna gain G_M given it is a near PB	$\beta_{M,f}$	conditional probability that SN_0 receives power from PB with antenna gain G_M given it is a far PB
P_p	transmit power per PB	P_s	aggregate received power from all PBs
$P_{s,n}$	aggregate received power from near PBs	$P_{s,f}$	aggregate received power from far PBs
$P_{s,n}^M$	aggregate received power from near PBs with G_M	$P_{s,f}^M$	aggregate received power from far PBs with G_M
$\mathbb{E}[P_s]$	expectation of P_s	$\mathbb{V}[P_s]$	variance of P_s
P_s^{omni}	aggregate received power from all omnidirectional PBs	P_s^{th}	received power threshold
F_s	sensor active probability	h_{X_i}	channel power gain between PB_i and SN_0

SN falls into this sector. Denote M as the random number of active sectors of a PB, e.g., PB_i, where $0 \leq M \leq N$. The adaptive beamforming strategy of PB_i is given as follows.

- SN's absence in charging region: If no sector of PB_i is active ($M = 0$), PB_i works as an omnidirectional antenna that radiates energy equally in all directions (to help charge SNs outside its charging region).
- SN's presence in charging region: If at least one sector of PB_i is active ($M \geq 1$), PB_i generates M equal-power energy beams in the directions of the M active sectors.

We use equal power allocation among the energy beams of a PB for the ease of analysis. In Section VI-C, we will show that equal power allocation is descent as compared with some other unequal allocation choices.

From an SN's point of view, the received power from the PBs is discussed as follows.

- Inside charging region (or within radius ρ): An SN can be intentionally and efficiently charged by one or more PBs whose charging regions cover its location.
- Outside charging region (or beyond radius ρ): When an SN is located outside the charging regions of the PBs, the SN still receives RF energy from the PBs if it is aligned with the energy radiation directions of the PBs.

We further explain the proposed AD-WPT scheme with the example of $N = 4$ in Fig. 1. It is observed that PB_1 detects three nearby sensors, i.e., SN_1, SN_2 and SN_3, which fall into three out of four sectors of its charging region. As a result, PB_1 adaptively generates three energy beams in the directions of north-east, north-west and south-west to directionally charge the three sensors. At the same time, PB_2 detects three sensors, i.e., SN_3, SN_4 and SN_5, which fall into two sectors of its charging region, and thus two adaptive energy beams are generated towards these SNs. In particular, notice that SN_3, which is within the overlapping area of the charging regions of PB_1 and PB_2, is thus intentionally charged by the two PBs at the same time. SN_1 is intentionally charged by PB_1 while it also receives energy from PB_2 and PB_3 since its location is aligned with the south-west energy radiation directions of these two PBs.

In this work, we focus on the analysis of the instantaneous received energy at the SNs in PBs' downlink energy transfer, which is a fundamental issue for all relevant works. To show the full picture, we introduce energy harvesting and consumption models for SNs as follows. A time-framed model is considered, where each time frame consists of energy harvesting slot (for energy harvesting from the PBs) and energy consumption slot (for periodic sensing and reporting tasks).[2] Due to the small-size and cost concerns in many sensors, we consider the SNs are not equipped with rechargeable batteries but capacitors.[3] During energy harvesting slot, the SNs receive energy from PBs via the AD-WPT scheme and charge their capacitors. If an SN receives enough energy to be active, it uses the received energy to perform sensing tasks and report data to the fusion centers during the energy consumption slot. Since capacitor can be charged and discharged quickly and can only store energy for a short period of time, we assume unit charging time and consider the energy in the capacitor is used up within the current time frame and cannot be carried forward to the next frame.[4] In Section VI-D, we further extend the results to the scenario with finite rechargeable battery, where SNs can store finite energy in the battery for future time frames' usage.

B. Antenna Gain under AD-WPT

When a PB is directional, the power intensity in the directions of energy beams improves compared with the case when the PB is omnidirectional. The ratio of power intensity between directional and omnidirectional antenna is defined as the gain of directional antenna G ($G \geq 1$) [26]. In the unintended directions of the directional PB, the power intensity

[2]We assume all nodes are synchronized and the node locations remain the same within a time frame.

[3]We consider each SN is equipped with a single antenna to receive RF signals from all possible directions, a rectifier to convert the RF signal to DC signal, and a capacitor to temporarily store the harvested energy.

[4]We assume the energy storage of the capacitors is sufficiently large (e.g., supercapacitors), where the SNs can use as much power as it receives in a time frame.

This article has been accepted for publication in a future issue of this journal, but has not been fully edited. Content may change prior to final publication. Citation information: DOI 10.1109/JSAC.2016.2551619, IEEE Journal on Selected Areas in Communications

is zero. In the following, we evaluate G given that M out of N sectors of the PB are active.

If none of the sectors of a PB is active ($M = 0$), as discussed, the PB behaves as an omnidirectional antenna with the uniform gain in all directions to help charge SNs outside its charging region,[5] i.e.,

$$G_M = 1, \text{ for } M = 0. \tag{1}$$

If M out of N sectors of the PB are active ($M \geq 1$), the PB forms M ($M \leq N$) energy beams with equal power in the direction of each beam.[6] By the law of conservation of energy, the total radiated power for directional and omnidirectional antenna is the same. Since the directional antenna concentrates the energy from the directions of N sectors into M sectors, the power intensity in the intended directions becomes N/M times of that of the omnidirectional antenna. Therefore, given M energy beams at the PB, the antenna gain in the direction of each energy beam is approximated as

$$G_M = N/M, \text{ for } M = 1, \cdots, N. \tag{2}$$

From (1) and (2), we see that the proposed AD-WPT is equivalent to the omnidirectional WPT with uniform gain when $M = 0$ or $M = N$.

Remark 1: The antenna gains and number of energy beams of the PBs are related to the charging radius ρ. As $\rho \to 0$, no SN is inside the charging regions ($M = 0$) and all PBs radiate energy in N directions with gain $G_0 = 1$ as omnidirectional WPT. As the increase of ρ, more sectors of the PB are likely to be activated due to the increased number of SNs inside the charging region. The number of beams that most PB radiate with decreases from N to 1 sharply and then increases from 1, 2, $\cdots$, to N. The corresponding antenna gain increases from $G_0 = 1$ to $G_1 = N$ and then decreases from $G_1 = N$, $G_2 = \frac{N}{2}$, $\cdots$, to $G_N = 1$. As $\rho \to \infty$, AD-WPT is again equivalent to omnidirectional WPT with $G_N = 1$ in all N directions. As we can see, there is a tradeoff between the antenna gain G_M and the number of beams of the PBs. When the PB concentrates energy on fewer beams, the power intensity of each beam increases but at the cost of charging fewer SNs. To address the above tradeoff, the optimal charging radius is crucial in the AD-WPT design and will be analyzed in Section IV and Section V for different SN network requirements.

C. Aggregate Received Power at a Typical SN

In this subsection, we discuss the aggregate received power at a typical SN from all PBs in the network, where the antenna gain G_M varies across PBs.

Consider a typical sensor node SN_0 at the origin $o = (0, 0)$ and an arbitrary PB_i at location X_i. The fading channel power gain between PB_i and SN_0 is denoted by h_{X_i}. We assume h_{X_i} is i.i.d. distributed either across different time frames for each PB or across different PB nodes in each time frame. Most of our derivations hold for general channel distribution and we use Rayleigh fading for simulation results throughout the paper. If PB_i radiates energy with gain G_M (for $M = 0, 1, \cdots, N$) towards SN_0, the received power at SN_0 from PB_i is [27]

$$P_s^i = P_p h_{X_i} G_M \sigma \left[\max\left(\|X_i\|/d_0, 1\right)\right]^{-\alpha}, \tag{3}$$

where P_p is the transmit power of PB_i, $\alpha > 2$ is the path loss exponent, σ is a unitless constant depending on the receiver energy convention efficiency and antenna characteristics.[7] The Euclidian distance between PB_i and SN_0 is represented by $\|X_i\|$, and d_0 is a reference distance for the antenna far field. We adopt the non-singular path loss model [7] to avoid $[\|X_i\|/d_0]^{-\alpha} > 1$ for $\|X_i\| < d_0$. Without loss of generality, we use $d_0 = 1$ m throughout the paper.

Equation (3) holds if PB_i radiates energy with gain G_M towards SN_0, where G_M is given in (1) or (2) depending on the number M of active sectors of PB_i. By considering all PBs in the network, the aggregate received power at SN_0 is

$$P_s = \sum_{X_i \in \Phi_p} P_s^i \mathbb{1}\left(\text{SN}_0 \text{ receives energy from } \text{PB}_i \text{ with } G_M\right).$$

The indicator function equals one if both the following conditions are satisfied:

- Condition 1: PB_i has M active sectors;
- Condition 2: SN_0 is in one of the M radiation directions of PB_i given PB_i has M active sectors.

We see that both conditions are related to the distance between SN_0 and PB_i. If SN_0 is inside the charging region of PB_i, SN_0 must be in the radiation direction of PB_i and M may vary from 1 to N. If SN_0 is outside the charging region of PB_i, SN_0 may not be in the radiation direction of PB_i and M may vary from 0 to N.

According to the distance between PB_i and SN_0, we classify the PBs into two groups: *near* PBs with $\|X_i\| \leq \rho$, and *far* PBs with $\|X_i\| > \rho$. We draw an equivalent charging region centered at SN_0 with radius ρ and denote $b(o, \rho)$ and $\overline{b(o, \rho)}$ as the regions inside and outside this charging region, respectively. We define two indicator functions $\theta_{M,n}$ and $\theta_{M,f}$ to describe the events that SN_0 receives power from the PB with G_M conditioned on this PB is a near PB or far PB, respectively, i.e.,

$$\theta_{M,n} = \mathbb{1}\left[\text{SN}_0 \text{ receives from } \text{PB}_i \text{ with } G_M \mid \|X_i\| \leq \rho\right]$$

and

$$\theta_{M,f} = \mathbb{1}\left[\text{SN}_0 \text{ receives from } \text{PB}_i \text{ with } G_M \mid \|X_i\| > \rho\right],$$

where subscript M denotes the number of active sectors of the PB and subscripts n and f denote the near and far PBs, respectively.

We denote $P_{s,n}$ as the aggregate received power from the near PBs and $P_{s,f}$ as the aggregate received power from the

[5]Besides improving SNs' power reception, this also helps keep the same total transmit power for AD-WPT and omnidirectional-WPT for fair comparison between them later.

[6]For simplicity, we assume the side lobes are negligible and the radiated energy is uniformly distributed across each energy beam.

[7]For empirical approximation, σ can be set to be the product of the energy conversion efficiency ζ and the free-space path loss at distance d_0 assuming omnidirectional antennas, i.e., $\sigma = 20 \log_{10} \frac{\sqrt{\zeta}\nu}{4\pi d_0}$ dB [27], where ν is the wavelength of the radio waves. For simplicity, we assume no energy conversion loss with $\zeta = 1$ throughout the paper.

This article has been accepted for publication in a future issue of this journal, but has not been fully edited. Content may change prior to final publication. Citation information: DOI 10.1109/JSAC.2016.2551619, IEEE Journal on Selected Areas in Communications

far PBs that radiate energy towards SN_0. By summing them up, we rewrite P_s as

$$P_s = P_{s,n} + P_{s,f}, \tag{4}$$

where

$$P_{s,n} = P_p \sigma \sum_{X_i \in \Phi_p \bigcap b(o,\rho)} h_{X_i} G_M \theta_{M,n} \left[\max\left(\|X_i\|, 1\right)\right]^{-\alpha}$$

and

$$P_{s,f} = P_p \sigma \sum_{X_i \in \Phi_p \bigcap \overline{b(o,\rho)}} h_{X_i} G_M \theta_{M,f} \left[\max\left(\|X_i\|, 1\right)\right]^{-\alpha}.$$

As a special case of $N = 1$, all PBs are omnidirectional radiators with gain of 1. The aggregate received power at SN_0 from all omnidirectional PBs is

$$P_s^{omni} = P_p \sigma \sum_{X_i \in \Phi_p} h_{X_i} \left[\max\left(\|X_i\|, 1\right)\right]^{-\alpha}. \tag{5}$$

III. Characterization of Received Power Distribution Using Stochastic Geometry

In this section, we analyze the distribution of aggregate received power at a typical SN from all PBs in the network using stochastic geometry.

To fully characterize the received power distribution, we usually use Laplace transform, which is however, difficult to be derived directly from (4). In the conditional events of $\theta_{M,n}$ and $\theta_{M,f}$, the gain G_M of PB_i is also related to the locations of other nearby SNs of PB_i which are unknown. Moreover, since G_M varies for each PB, the PBs that radiate power with G_M towards SN_0 can be regarded as a heterogeneous network for which the Laplace transform is hard to characterize. In the following discussions, we use an alternative method by utilizing the independent thinning [7] of the network. For the near PBs and the far PBs, respectively, we thin the heterogeneous network into multiple homogeneous networks with certain probabilities, where in each homogeneous network the PBs radiate energy towards SN_0 with the same gain G_M. We have $M = 1, \cdots, N$ for the near PBs and $M = 0, 1, \cdots, N$ for the far PBs. After analyzing the Laplace transform of the received power distribution in each homogeneous network, we finally derive the distribution metrics of the aggregate received power from all PBs at SN_0.

A. Power Reception Probability given PB Location

First, we derive the thinning probabilities of the near PBs and the far PBs. As discussed previously, SN_0 receives power from PB_i with gain G_M if both Conditions 1 and 2 are satisfied. As for Condition 1, PB_i transmits with gain G_M if it has M active sectors. We derive the active probability of each sector as follows. As SNs follow PPP with density λ_s, the number of SNs inside a charging region is a Poisson random variable with mean $\lambda_s \pi \rho^2$. When the charging region is equally partitioned into N sectors, the number of SNs inside one of these N sectors is also a Poisson random variable, denoted by l, with mean $\lambda_s \pi \rho^2 / N$, and the probability mass function is given by

$$\Pr\left(l = \kappa\right) = \frac{\left(\lambda_s \pi \rho^2 / N\right)^{\kappa}}{\kappa!} \exp\left(-\lambda_s \pi \rho^2 / N\right), \ \kappa = 0, 1, \cdots$$

The probability that no SN is inside a sector is thus

$$p = \Pr\left(l = 0\right) = \exp\left(-\lambda_s \pi \rho^2 / N\right). \tag{6}$$

Therefore, the active probability of a sector is the probability that at least one SN is inside this sector, which is given by

$$q = 1 - p = 1 - \exp\left(-\lambda_s \pi \rho^2 / N\right). \tag{7}$$

Denote $\beta_{M,n}$ and $\beta_{M,f}$ as the conditional probabilities that SN_0 receives energy from PB_i with antenna gain G_M given PB_i is a near PB and a far PB, respectively. Based on p, q, Conditions 1 and 2, we derive $\beta_{M,n}$ and $\beta_{M,f}$ as follows.

1) Near PBs: If $\|X_i\| \leq \rho$, PB_i radiates energy in at least the direction towards SN_0 ($M \geq 1$). Condition 2 is thus satisfied. Given PB_i is a near PB, the conditional probability that PB_i radiates with gain G_M is

$$\omega_{M,n} = \binom{N-1}{M-1} p^{N-M} q^{M-1}, \tag{8}$$

which is the probability that the rest $M-1$ out of $N-1$ sectors of PB_i have SNs. Given PB_i is a near PB that radiates with gain G_M, the conditional probability that SN_0 receives energy from PB_i is

$$\varphi_{M,n} = 1. \tag{9}$$

Since $\beta_{M,n} = \varphi_{M,n} \omega_{M,n}$, we obtain the following lemma.

Lemma 1: Given PB_i is a near PB, the conditional probability that SN_0 receives energy from PB_i with gain G_M is

$$\beta_{M,n} = \binom{N-1}{M-1} p^{N-M} q^{M-1}, \text{ for } M = 1, \cdots, N. \tag{10}$$

2) Far PBs: If $\|X_i\| > \rho$, PB_i may not radiate energy towards SN_0 ($M = 0, \cdots, N$). SN_0 receives energy from PB_i with G_M if both Conditions 1 and 2 are satisfied. Given PB_i is a far PB, the conditional probability that PB_i radiates with gain G_M is

$$\omega_{M,f} = \begin{cases} p^N, & \text{for } M = 0 \quad (11a) \\ \binom{N}{M} p^{N-M} q^M, & \text{for } M = 1, \cdots, N. \quad (11b) \end{cases}$$

Given PB_i is a far PB that radiates with gain G_M, the conditional probability that SN_0 receives energy from PB_i is

$$\varphi_{M,f} = \begin{cases} 1, & \text{for } M = 0 \quad (12a) \\ \dfrac{M}{N}, & \text{for } M = 1, \cdots, N. \quad (12b) \end{cases}$$

Since $\beta_{M,f} = \varphi_{M,f} \omega_{M,f}$, we obtain the following lemma.

Lemma 2: Given PB_i is a far PB, the conditional probability that SN_0 receives energy from PB_i with gain G_M is

$$\beta_{M,f} = \begin{cases} p^N, & \text{for } M = 0 \\ \binom{N-1}{M-1} p^{N-M} q^M, & \text{for } M = 1, \cdots, N. \end{cases}$$

This article has been accepted for publication in a future issue of this journal, but has not been fully edited. Content may change prior to final publication. Citation information: DOI 10.1109/JSAC.2016.2551619, IEEE Journal on Selected Areas in Communications

B. Characterization of Received Power via Laplace Transform

Define the Laplace transform of the distribution of P_s as $\mathcal{L}_{P_s}(s) = \mathbb{E}\left[\exp\left(-sP_s\right)\right]$. In this subsection, we derive the Laplace transform $\mathcal{L}_{P_s}(s)$ to characterize the received power at the typical SN_0.

We denote Φ_p^M as the subset of PBs with gain G_M and $\Phi_p^{'}$ as the subset of PBs that radiate energy towards SN_0. The subset of near PBs within $b(o,\rho)$ that radiate energy with gain G_M towards SN_0 is

$$\Phi_{p,n}^M = \Phi_p^M \bigcap \Phi_p^{'} \bigcap b(o,\rho), \text{ for } M = 1, \cdots, N, \quad (14)$$

which is obtained through the independent thinning [7] of near PBs with new density $\lambda_p \beta_{M,n}$, where $\beta_{M,n}$ is given in Lemma 1. The near PBs can be regarded as a heterogeneous network consisting of a group of homogeneous networks each with antenna gain G_M and density $\lambda_p \beta_{M,n}$. Similarly, the subset of far PBs within $\overline{b(o,\rho)}$ that radiate energy with gain G_M towards SN_0 is

$$\Phi_{p,f}^M = \Phi_p^M \bigcap \Phi_p^{'} \bigcap \overline{b(o,\rho)}, \text{ for } M = 0, \cdots, N, \quad (15)$$

which is obtained by the independent thinning of far PBs with new density $\lambda_p \beta_{M,f}$, where $\beta_{M,f}$ is given in Lemma 2. The far PBs that radiate power towards SN_0 can be regarded as another heterogeneous network consisting of a group of homogeneous networks each with gain G_M and density $\lambda_p \beta_{M,f}$. Note that SN_0 receives zero power from the far PBs that does not radiate energy towards SN_0. In the following, we derive the Laplace transform of the received power distribution in each homogeneous network, and then derive that of the aggregate received power from all PBs.

We rewrite the aggregate received power at SN_0 from all the near PBs and far PBs in (4) as

$$P_s = P_{s,n} + P_{s,f} = \sum_{M=1}^{N} P_{s,n}^M + \sum_{M=0}^{N} P_{s,f}^M, \quad (16)$$

where

$$P_{s,n}^M = P_p \sigma \sum_{X_i \in \Phi_{p,n}^M} h_{X_i} G_M \left[\max\left(\|X_i\|, 1\right)\right]^{-\alpha} \quad (17)$$

is the aggregate received power from the near PBs with gain G_M and

$$P_{s,f}^M = P_p \sigma \sum_{X_i \in \Phi_{p,f}^M} h_{X_i} G_M \left[\max\left(\|X_i\|, 1\right)\right]^{-\alpha} \quad (18)$$

is the aggregate received power from the far PBs with gain G_M. Since we adopt the non-singular path loss function $\left[\max\left(\|X_i\|, 1\right)\right]^{-\alpha}$, our analysis involves two cases: $0 < \rho \leq 1$ and $1 < \rho < \infty$. Define $\gamma(s,x) = \int_0^x t^{s-1} e^{-t} dt$ as the lower incomplete gamma function. The Laplace transforms of the distributions of $P_{s,n}^M$ and $P_{s,f}^M$ are given as follows.

Lemma 3: The Laplace transform of the distribution of aggregate received power at the typical SN_0 from the near PBs with gain G_M is

$$\mathcal{L}_{P_{s,n}^M}(s) = \begin{cases} \mathcal{L}_{P_{s,n}^M(1)}(s), \text{ for } 0 < \rho \leq 1 & (19a) \\ \mathcal{L}_{P_{s,n}^M(2)}(s), \text{ for } 1 < \rho < \infty, & (19b) \end{cases}$$

where

$$\mathcal{L}_{P_{s,n}^M(1)}(s) = \exp\Big[-\lambda_p \pi \beta_{M,n} \rho^2 \times \mathbb{E}_{h_{X_i}}\Big[1 - \exp\left(-sP_p \sigma h_{X_i} G_M\right)\Big]\Big]$$

and

$$\mathcal{L}_{P_{s,n}^M(2)}(s) = \exp\Bigg[-\lambda_p \pi \beta_{M,n} \Bigg[\rho^2 \mathbb{E}_{h_{X_i}}\Big[1 - \exp\left(-sP_p \sigma h_{X_i} G_M \rho^{-\alpha}\right)\Big] + \mathbb{E}_{h_{X_i}}\Big[\left(sP_p \sigma h_{X_i} G_M\right)^{\frac{2}{\alpha}} \left[\gamma\left(1 - 2/\alpha, sP_p \sigma h_{X_i} G_M\right) - \gamma\left(1 - 2/\alpha, sP_p \sigma h_{X_i} G_M \rho^{-\alpha}\right)\right]\Big]\Bigg]\Bigg].$$

Proof: See Appendix A. ∎

Lemma 4: The Laplace transform of the distribution of aggregate received power at the typical SN_0 from the far PBs with gain G_M is

$$\mathcal{L}_{P_{s,f}^M}(s) = \begin{cases} \mathcal{L}_{P_{s,f}^M(1)}(s), \text{ for } 0 < \rho \leq 1 & (20a) \\ \mathcal{L}_{P_{s,f}^M(2)}(s), \text{ for } 1 < \rho < \infty, & (20b) \end{cases}$$

where

$$\mathcal{L}_{P_{s,f}^M(1)}(s) = \exp\Bigg[\lambda_p \pi \beta_{M,f} \Bigg[\rho^2 \mathbb{E}_{h_{X_i}}\left[1 - \exp\left(-sP_p \sigma h_{X_i} G_M\right)\right] - \mathbb{E}_{h_{X_i}}\left[\left(sP_p \sigma h_{X_i} G_M\right)^{\frac{2}{\alpha}} \gamma\left(1 - 2/\alpha, sP_p \sigma h_{X_i} G_M\right)\right]\Bigg]\Bigg]$$

and

$$\mathcal{L}_{P_{s,f}^M(2)}(s) = \exp\Bigg[\lambda_p \pi \beta_{M,f} \Bigg[\rho^2 \mathbb{E}_{h_{X_i}}\left[1 - \exp\left(-sP_p \sigma h_{X_i} G_M \rho^{-\alpha}\right)\right] - \mathbb{E}_{h_{X_i}}\left[\left(sP_p \sigma h_{X_i} G_M\right)^{\frac{2}{\alpha}} \gamma\left(1 - 2/\alpha, sP_p \sigma h_{X_i} G_M \rho^{-\alpha}\right)\right]\Bigg]\Bigg].$$

Proof: The proof is similar to that of Lemma 3 and is omitted for brevity. ∎

Based on Lemma 3 and Lemma 4, we obtain the Laplace transform of the distribution of P_s in the following proposition.

Proposition 1: The Laplace transform of the distribution of aggregate received power at the typical SN_0 from all PBs under AD-WPT is given by

$$\mathcal{L}_{P_s}(s) = \begin{cases} \prod_{M=1}^{N} \mathcal{L}_{P_{s,n}^M(1)}(s) \prod_{M=0}^{N} \mathcal{L}_{P_{s,f}^M(1)}(s), \ 0 < \rho \leq 1 \\ \prod_{M=1}^{N} \mathcal{L}_{P_{s,n}^M(2)}(s) \prod_{M=0}^{N} \mathcal{L}_{P_{s,f}^M(2)}(s), \ 1 < \rho < \infty. \end{cases}$$

As a special case of $N = 1$, the Laplace transform of the distribution of aggregate received power at SN_0 from all PBs in omnidirectional WPT is given by

$$\mathcal{L}_{P_s^{omni}}(s) = \exp\Bigg[-\lambda_p \pi \mathbb{E}_{h_{X_i}}\Bigg[\left(sP_p \sigma h_{X_i}\right)^{\frac{2}{\alpha}} \times \gamma\left(1 - \frac{2}{\alpha}, sP_p \sigma h_{X_i}\right)\Bigg]\Bigg]. \quad (22)$$

This article has been accepted for publication in a future issue of this journal, but has not been fully edited. Content may change prior to final publication. Citation information: DOI 10.1109/JSAC.2016.2551619, IEEE Journal on Selected Areas in Communications

Proof:

$$\begin{aligned}\mathcal{L}_{P_s}(s) &= \mathbb{E}\left[\exp\left(-sP_s\right)\right] \\ &= \mathbb{E}\left[\exp\left(-s\left(P_{s,n}+P_{s,f}\right)\right)\right] \\ &= \mathbb{E}\left[\exp\left(-sP_{s,n}\right)\right]\mathbb{E}\left[\exp\left(-sP_{s,f}\right)\right] \\ &= \mathbb{E}\left[\exp\left(-s\sum_{M=1}^{N}P_{s,n}^{M}\right)\right]\mathbb{E}\left[\exp\left(-s\sum_{M=0}^{N}P_{s,f}^{M}\right)\right] \\ &= \prod_{M=1}^{N}\mathcal{L}_{P_{s,n}^{M}}(s)\prod_{M=0}^{N}\mathcal{L}_{P_{s,f}^{M}}(s). \end{aligned} \tag{23}$$

Substituting $\mathcal{L}_{P_{s,n}^{M}}(s)$ in Lemma 3 and $\mathcal{L}_{P_{s,f}^{M}}(s)$ in Lemma 4 into (23), we obtain the Laplace transform given in Proposition 1. It is noted that $\mathcal{L}_{P_s}(s)$ is continuous at $\rho=1$. ∎

Corollary 1: For $\rho \to 0$ or $\rho \to \infty$, we have $\mathcal{L}_{P_s}(s) \to \mathcal{L}_{P_s^{omni}}(s)$.

Proof: See Appendix B. ∎

From Corollary 1, we see that the AD-WPT is equivalent to omnidirectional WPT for $\rho \to 0$ or $\rho \to \infty$ even with $N > 1$.

C. Mean, Variance and CCDF of Received Power

We derive the closed-form mean and variance of the received power at SN_0 based on the first and second cumulants of P_s [28, Definition 5.302]. An alternative method is by using Campbell's theorem and the second-order product density as introduced in [7, Theorem A.2, Definition A.4 and Lemma A.3].

Taking the first cumulant of P_s [7, Eqn. (3.44)], the average received power at SN_0 is given by

$$\mathbb{E}[P_s] = -\frac{d}{ds}\left[\log\left(\mathcal{L}_{P_s}(s)\right)\right]|_{s=0}. \tag{24}$$

This is the expectation of the aggregate received power at SN_0 from all PBs by taking over all possible location realizations of the PBs in spatial domain. By further derivations, the results are summarized in the following proposition.

Proposition 2: At the typical SN_0, the average received power in AD-WPT is given by

$$\mathbb{E}\left[P_s\right] = \begin{cases} P_p\lambda_p\sigma\pi\mathbb{E}\left[h_{X_i}\right]\left[\dfrac{\rho^2\left(p-p^N\right)}{1-p}+\dfrac{\alpha}{\alpha-2}\right], \\ \qquad\qquad \text{for } 0<\rho\le 1 \quad \text{(25a)} \\ P_p\lambda_p\sigma\pi\mathbb{E}\left[h_{X_i}\right]\left[\dfrac{\left(\alpha-2\rho^{2-\alpha}\right)\left(1-p^N\right)}{(\alpha-2)(1-p)}\right. \\ \qquad\left.+\dfrac{2\rho^{2-\alpha}}{\alpha-2}\right], \text{ for } 1<\rho<\infty \quad \text{(25b)} \end{cases}$$

where p is given in (6) and $\mathbb{E}(P_s)$ is continuous at $\rho=1$. As a special case of $N=1$, the average received power at SN_0 in omnidirectional WPT is given by

$$\mathbb{E}[P_s^{omni}] = \frac{P_p\lambda_p\sigma\pi\alpha\mathbb{E}\left[h_{X_i}\right]}{\alpha-2}. \tag{26}$$

Proof: See Appendix C. With $N=1$, both (25a) and (25b) equal (26) for all ρ. ∎

In Rayleigh fading with $h_{X_i} \sim \exp(-h_{X_i})$, we have $\mathbb{E}\left[h_{X_i}\right]=1$. The average received power is thus the same as that in the non-fading case. This is because the good and bad channels on average offset each other. In Proposition 2, for any given ρ, $\mathbb{E}[P_s]$ is increasing with the increased P_p, λ_p and N, and it is decreasing with the increased λ_s. Moreover, for any given set of $\{P_p, \lambda_p, \lambda_s, N\}$, we observe that $\mathbb{E}[P_s]$ is unimodal in ρ, i.e., there exists an optimal ρ^* that maximizes $\mathbb{E}[P_s]$, where $\mathbb{E}[P_s]$ is monotonically increasing for $\rho \le \rho^*$ and is monotonically decreasing for $\rho \ge \rho^*$. We will further analyze the optimal ρ^* in Section IV.

The comparison of the average received power between AD-WPT ($N>1$) and omnidirectional WPT ($N=1$) is given in the following corollaries.

Corollary 2: For $0<\rho<\infty$, it follows that $\mathbb{E}[P_s] > \mathbb{E}[P_s^{omni}]$. For $\rho \to 0$ and $\rho \to \infty$, we have $\mathbb{E}[P_s] \to \mathbb{E}[P_s^{omni}]$.

Proof: See Appendix D. ∎

From Corollary 2, we see that the average received power at SN_0 from all PBs in AD-WPT is higher than that in omnidirectional WPT with any strictly positive and finite ρ. Next, we further discuss how the near PBs ($\|X_i\| \le \rho$) and far PBs ($\|X_i\| > \rho$) influence the average received power. For comparison, we denote the aggregate received power from the PBs with $\|X_i\| \le \rho$ and $\|X_i\| > \rho$ in omnidirectional WPT by $P_{s,n}^{omni}$ and $P_{s,f}^{omni}$, respectively.

Corollary 3: The ratio of the average received power at SN_0 from the near PBs in AD-WPT ($N>1$) and that in omnidirectional WPT ($N=1$) is given by

$$\frac{\mathbb{E}[P_{s,n}]}{\mathbb{E}[P_{s,n}^{omni}]} = \frac{1-p^N}{1-p} > 1 \tag{27}$$

The ratio of the average received power at SN_0 from the far PBs in AD-WPT and in omnidirectional WPT is given by

$$\frac{\mathbb{E}[P_{s,f}]}{\mathbb{E}[P_{s,f}^{omni}]} = 1. \tag{28}$$

Proof: The proof is similar to that of Proposition 2 and thus omitted. ∎

In Corollary 3, we see that the average received power at SN_0 from the near PBs and far PBs in AD-WPT is greater than and equal to that in omnidirectional WPT as shown in (27) and (28), respectively. The improvement of the average received power from all PBs at SN_0 is thus due to the adaptive energy beamforming of the near PBs.

Taking the second cumulant of P_s [7, Eqn. (3.45)], we obtain the variance of the received power at SN_0, i.e.,

$$\mathbb{V}[P_s] = \frac{d^2}{ds^2}\left[\log\left(\mathcal{L}_{P_s}(s)\right)\right]|_{s=0}. \tag{29}$$

By further derivations, we summarize the results in the following proposition.

Proposition 3: At the typical SN_0, the variance of the received power in AD-WPT is given by (30a) and (30b), where $\mathbb{V}(P_s)$ is continuous at $\rho=1$. As a special case of $N=1$, the variance of the received power in omnidirectional WPT is

$$\mathbb{V}[P_s^{omni}] = \frac{\lambda_p P_p^2\sigma^2\pi\alpha\mathbb{E}\left[\left(h_{X_i}\right)^2\right]}{\alpha-1}. \tag{31}$$

This article has been accepted for publication in a future issue of this journal, but has not been fully edited. Content may change prior to final publication. Citation information: DOI 10.1109/JSAC.2016.2551619, IEEE Journal on Selected Areas in Communications

$$\mathbb{V}[P_s] = \begin{cases} \lambda_p P_p^2 \sigma^2 \pi \mathbb{E}\left[(h_{X_i})^2\right] \left[\left[\frac{\alpha}{\alpha-1} - \rho^2\right] p^N + \left[\left(q^{-1}-1\right)\rho^2 + \frac{\alpha}{\alpha-1}\right] \sum_{M=1}^{N} \left(\frac{N}{M}\right)^2 \binom{N-1}{M-1} p^{N-M} q^M\right], & \text{for } 0 < \rho \leq 1 \quad (30a) \\ \lambda_p P_p^2 \sigma^2 \pi \mathbb{E}\left[(h_{X_i})^2\right] \left[\frac{\rho^{2-2\alpha}}{\alpha-1} p^N + \left[\frac{\alpha-\rho^{2-2\alpha}}{\alpha-1} q^{-1} + \frac{\rho^{2-2\alpha}}{\alpha-1}\right] \sum_{M=1}^{N} \left(\frac{N}{M}\right)^2 \binom{N-1}{M-1} p^{N-M} q^M\right], & \text{for } 1 < \rho < \infty \quad (30b) \end{cases}$$

Proof: See Appendix E. With $N = 1$, (30a) and (30b) are the same and equal (31) for all ρ. ∎

In Rayleigh fading with $h_{X_i} \sim \exp(-h_{X_i})$, we have $\mathbb{E}\left[(h_{X_i})^2\right] = 2$. The variance of received power is thus twice as that in the non-fading case. Intuitively, the fluctuation of the received power increases due to the fading channel fluctuation.

According to (30a) and (30b), we observe that $\mathbb{V}[P_s]$ is unimodal in ρ, i.e., $\mathbb{V}[P_s]$ is first increasing and then decreasing with the increased ρ. Given any ρ, $\mathbb{V}[P_s]$ is increasing with P_p, λ_p and N, and it is decreasing with λ_s. We also compare the variance of the received power at SN_0 between AD-WPT ($N > 1$) and omnidirectional WPT ($N = 1$) in the following corollary.

Corollary 4: For $0 < \rho < \infty$, it follows that $\mathbb{V}[P_s] > \mathbb{V}[P_s^{omni}]$. For $\rho \to 0$ and $\rho \to \infty$, we have $\mathbb{V}[P_s] \to \mathbb{V}[P_s^{omni}]$.

Proof: The proof is similar to that of Corollary 2 and thus omitted. ∎

From Corollary 4, we see that the variance of received power in AD-WPT is higher than that in omnidirectional WPT. Though AD-WPT improves the average received power compared with omnidirectional WPT, it also leads to more significant spatial power fluctuation.

Next, we study the CCDF F_s of the received power at the typical SN_0, which is the probability that P_s takes on a value greater than or equal to a given threshold $P_s^{th} > 0$, i.e.,

$$F_s = \Pr\left(P_s \geq P_s^{th}\right) = \int_{P_s^{th}}^{\infty} f(P_s) dP_s, \quad (32)$$

where $f(P_s)$ is the probability density function (PDF) of P_s and can be calculated from the inverse Laplace transform of $\mathcal{L}_{P_s}(s)$ in Proposition 1, i.e.,

$$f(P_s) = \mathcal{L}_{P_s}^{-1}(s). \quad (33)$$

In some scenarios, an SN is active if the received power is beyond the constant operational power threshold P_s^{th} (e.g., minimum circuit activation power). Then, the CCDF of P_s can be regarded as the active probability of the SNs. Since F_s is increasing with $\mathbb{E}[P_s]$ and decreasing with $\mathbb{V}[P_s]$, the increased average received power and power fluctuation may improve or reduce the sensor active probability, respectively. As shown in Propositions 2 and 3, both $\mathbb{E}[P_s]$ and $\mathbb{V}[P_s]$ first increase and then decrease with the increased ρ. We will further discuss the above tradeoff and derive the optimal ρ^* that maximizes the sensor active probability in Section V.

IV. Maximization of Average Received Power in AD-WPT

In flexible-task WSN applications, each SN is assigned with flexible sensing tasks depending on the received energy, i.e., the SNs with high received power may handle more tasks than the low-power SNs for the benefit of the whole network. For example, the high-power SNs in a hierarchical network may work as cluster-heads [1] that collect data from the low-power SNs and coordinate sensing tasks among the SNs. The low-power SNs can also offload part of the computational processing tasks to the high-power SNs which have more available resource. To achieve energy efficient AD-WPT in flexible-task WSN, it is important to maximize the total received power over all SNs, which is equivalent to maximizing the average received power at the typical SN_0. In this section, we design the optimal charging radius ρ^* for maximizing $\mathbb{E}[P_s]$ in Proposition 2.

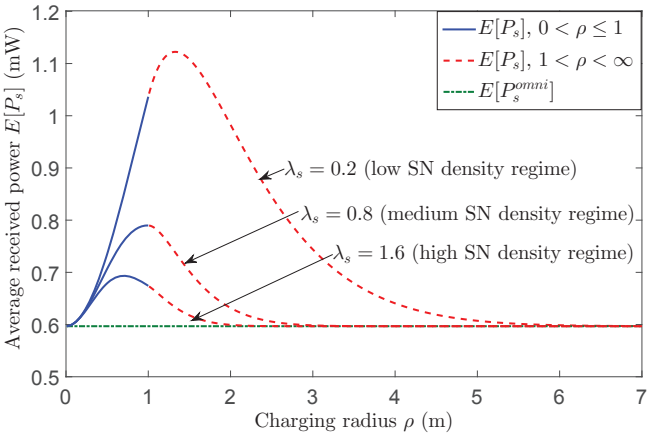

Fig. 2. Average received power versus charging radius ($P_p = 10$ W, $\nu = 0.1$ m, $\alpha = 3$, $\lambda_p = 0.1$ nodes/m^2 and $N = 4$).

A. Effect of Power Intensity and Power Opportunity

In Fig. 2, the average received power in AD-WPT $\mathbb{E}[P_s]$ is shown to be unimodal in ρ and outperform that of $\mathbb{E}[P_s^{omni}]$ in omnidirectional WPT, as stated in Proposition 2 and Corollary 1. The received power at SN_0 from PB_i depends on three factors: whether PB_i radiates power towards SN_0, the intensity of the radiated energy, and the channel fading gain h_{X_i}, where the first two factors can be viewed as the power opportunity and power intensity of the PB, respectively. As we discussed in Section III-C, the Rayleigh fading does not influence the average received power, we therefore focus on the first two factors by considering the non-fading case in the following discussions. Since both the power opportunity and power intensity are related to the number of beams of PB_i and the distance $\|X_i\|$ between PB_i and SN_0, we discuss the average received power at SN_0 from the near PBs ($\|X_i\| \leq \rho$) and far PBs ($\|X_i\| > \rho$) as follows.

This article has been accepted for publication in a future issue of this journal, but has not been fully edited. Content may change prior to final publication. Citation information: DOI 10.1109/JSAC.2016.2551619, IEEE Journal on Selected Areas in Communications

- *Near PBs*: The average received power from the near PBs in AD-WPT is higher than that in omnidirectional WPT (see (27) in Corollary 2). When the number of beams from a near PB decreases, the power intensity of this near PB increases (see (2)), and the power opportunity that the near PB radiates power towards SN_0 is with probability 1 since the near PB forms at least one beam towards SN_0.
- *Far PBs*: The average received power from the far PBs in AD-WPT is the same as that in omnidirectional WPT (see (28) in Corollary 2). When the number of beams of a far PB decreases, the power intensity of this far PB increases (see (1) and (2)), but the power opportunity that SN_0 receives energy from this far PBs decreases (see (12a) and (12b)), and vice versa. From the average perspective, the effects of power intensity and power opportunity of the far PBs cancel with each other.

From the above discussions, $\mathbb{E}[P_s]$ outperforms $\mathbb{E}[P_s^{omni}]$ mainly because of the high power intensity from the near PBs. We discuss $\mathbb{E}[P_s]$ as follows.

- As $\rho \to 0$, no SN is in the charging regions. $\mathbb{E}[P_s]$ is equivalent to $\mathbb{E}[P_s^{omni}]$ since all PBs radiate power in N directions.
- As ρ increases, a small number of SNs are included in the charging regions and the PBs that are close to SN_0 become near PBs. When most PBs concentrate the transmit power from N beams into 1 beam, the power intensity is greatly enhanced compared with omnidirectional WPT. $\mathbb{E}[P_s]$ increases with the increased ρ due to the increased number of the near PBs and increased power intensity of the PBs.
- As ρ further increases, more sectors of the PBs are likely to be activated due to the increased number of SNs in the charging regions. When the number of beams of most PBs increases from 1, 2, $\cdots$, to N, the power intensity for each beam decreases. There is a tradeoff between the further increased number of the near PBs and the decreased power intensity. $\mathbb{E}[P_s]$ thus increases and then decreases with the increased ρ.
- As $\rho \to \infty$, all SNs are in the charging regions and AD-WPT is again equivalent to omnidirectional WPT.

B. Optimal Charging Radius for Average Power Maximization

In the following, we study the optimal charging radius ρ^* that maximizes $\mathbb{E}[P_s]$ in Proposition 2, i.e.,

$$\text{P1}: \quad \mathbb{E}[P_s]^* = \max_{0<\rho<\infty} \mathbb{E}[P_s]. \tag{34}$$

In Fig. 2, for omnidirectional WPT, $\mathbb{E}[P_s^{omni}]$ is regardless of λ_s which matches with (26). This is because each PB radiates energy in all directions without catering to the locations or density of the SNs. For AD-WPT, $\mathbb{E}[P_s]$ decreases with the increased λ_s. With the increased number of SNs in the charging regions, PBs are more likely to radiate with more beams and less power intensity, which thus reduces the average received power at SN_0. In the following, we discuss the optimal ρ^* for different λ_s under AD-WPT in Rayleigh fading.

Case 1: Low SN Density Regime. When the SN network density is low, e.g., $\lambda_s = 0.2$ in Fig. 2, we have $\frac{\partial \mathbb{E}[P_s]}{\partial \rho}|_{\rho=1} > 0$. Since (25b) is unimodal in ρ and (25a) is an increasing function of ρ, the optimal charging radius $\rho^* \in (1, \infty)$ is the stationary point of (25b). Taking the first derivative of (25b) with respect to ρ, we have

$$\frac{\partial \left[\mathbb{E}[P_s]|_{1<\rho<\infty}\right]}{\partial \rho} = 2P_p\lambda_p\pi\sigma\left[\frac{\rho^{1-\alpha}\left(p-p^N\right)}{1-p} + \frac{\lambda_s\pi p^N\rho\left(\alpha-2\rho^{2-\alpha}\right)}{(\alpha-2)(1-p)} - \frac{\lambda_s\pi\rho p\left(\alpha-2\rho^{2-\alpha}\right)\left(1-p^N\right)}{(1-p)^2(\alpha-2)N}\right].$$

The optimal charging radius ρ^* is the unique solution of $\frac{\partial[\mathbb{E}[P_s]|_{1<\rho<\infty}]}{\partial \rho} = 0$. Though ρ^* is not analytically tractable, we can search it numerically using one-dimensional searching method.

Case 2: Medium SN Density Regime. When the SN network has a medium density, e.g., $\lambda_s = 0.8$ in Fig. 2, we have $\frac{\partial \mathbb{E}[P_s]}{\partial \rho}|_{\rho=1} = 0$. In this case, (25a) is an increasing function of ρ and (25b) is a decreasing function of ρ. The optimal charging region radius is at the point of $\rho^* = 1$.

Case 3: High SN Density Regime. When the SN network has a high density, e.g., $\lambda_s = 1.6$ in Fig. 2, we have $\frac{\partial \mathbb{E}[P_s]}{\partial \rho}|_{\rho=1} < 0$. In this case, (25a) is unimodal in ρ and (25b) is a decreasing function of ρ. The optimal charging radius $\rho^* \in (0, 1)$ is the stationary point of (25a). Taking the first derivative of (25a), we have

$$\frac{\partial \left[\mathbb{E}[P_s]|_{0<\rho\leq 1}\right]}{\partial \rho} = 2P_p\lambda_p\pi\sigma\left[\frac{\lambda_s\pi\rho^3 p(p^N-p)}{N(1-p)^2} + \frac{\rho(p-p^N)+\lambda_s\pi\rho^3 p\left(p^{N-1}-\frac{1}{N}\right)}{1-p}\right]. \tag{35}$$

The optimal charging radius ρ^* is the unique solution to $\frac{\partial\left[\mathbb{E}[P_s]|_{0<\rho\leq 1}\right]}{\partial \rho} = 0$. Similar to Case 1, ρ^* is not analytically tractable but can be searched numerically.

It can be proved that $\frac{\partial\left[\mathbb{E}[P_s]|_{0<\rho\leq 1}\right]}{\partial \rho}$ and $\frac{\partial[\mathbb{E}[P_s]|_{1<\rho<\infty}]}{\partial \rho}$ are of the same sign at the point of $\rho = 1$. The procedure of obtaining the optimal ρ^* is summarized in Algorithm 1. More numerical results will be shown in Section VI-A.

Algorithm 1 Solving the optimal charging radius in P1:

1: Calculate $D_1(\rho) = \frac{\partial\left[\mathbb{E}[P_s]|_{0<\rho\leq 1}\right]}{\partial \rho}$ and $D_2(\rho) = \frac{\partial[\mathbb{E}[P_s]|_{1<\rho<\infty}]}{\partial \rho}$
2: **if** either $D_1(\rho=1) < 0$ or $D_2(\rho=1) < 0$ **then**
3: $\quad \rho^*$ is the solution to $D_1(\rho) = 0$
4: **else if** either $D_1(\rho=1) = 0$ or $D_2(\rho=1) = 0$ **then**
5: $\quad \rho^* = 1$
6: **else if** either $D_1(\rho=1) > 0$ or $D_2(\rho=1) > 0$ **then**
7: $\quad \rho^*$ is the solution to $D_2(\rho) = 0$
8: **end if**

V. Maximization of Sensor Active Probability in AD-WPT

In the previous section, we discussed the optimal AD-WPT design in flexible-task WSN scenario where the energy consumption levels or tasks vary for different SNs. In

This article has been accepted for publication in a future issue of this journal, but has not been fully edited. Content may change prior to final publication. Citation information: DOI 10.1109/JSAC.2016.2551619, IEEE Journal on Selected Areas in Communications

some other scenarios, e.g., environmental measurement and surveillance monitoring systems, the sensing information from each SN is equally important and mutually irreplaceable. For example, in a forest fire detection system [1], SNs are randomly deployed in a forest collecting temperature and humidity data independently. In this case, there is certain energy cost requirement [29] at SNs to fulfill equal amount of sensing, transmission and other basic processing tasks, which requires a fixed operational power threshold. Another practical concern is power sensitivity, where the RF energy harvesting circuit is activated only if the received power from energy transfer is greater than a certain threshold (see, e.g., [3]). In this section, we consider the case that SN has a minimum operational power requirement, i.e., an SN is active only if the received power is beyond the target energy threshold P_s^{th}. We analyze the optimal charging radius ρ^* in AD-WPT to maximize the active probability F_s of the SNs.

A. Effect of Power Intensity and Power Opportunity

As discussed in Section IV, the decreased number of beams at the PBs improves the radiated power intensity, which enhances the average received power at SN_0 in AD-WPT compared with omnidirectional WPT. However, the decreased number of beams may not enhance the sensor active probability F_s due to the interplay between the power intensity and power opportunity. First, we discuss the effect of power intensity and power opportunity in non-fading case.

- *Near PBs*: The near PBs help improve the sensor active probability in AD-WPT compared with that in omnidirectional WPT. Since the near PBs always radiate energy towards SN_0 with probability 1 (see (9)) and antenna gain greater than 1 (see (2)), the received power from the near PBs in AD-WPT is higher than that in omnidirectional WPT. With the decreased number of beams from the near PBs, the power intensity increases, which increases the received power from the near PBs and may improve the sensor active probability in AD-WPT.
- *Far PBs*: The far PBs can reduce the sensor active probability in AD-WPT compared with that in omnidirectional WPT. Since the far PBs may not radiate energy towards SN_0, the received power from a far PB in AD-WPT is higher than that in omnidirectional WPT or zero if SN_0 is inside or outside the beamforming directions of the PB, respectively. With the decreased number of beams from the far PBs, the power intensity of the far PBs increases (see (1) and (2)), but the power opportunity to receive energy from the far PBs at SN_0 decreases (see (12a) and (12b)). Since SN_0 has a higher chance to fall outside the radiation directions of the far PBs, the received power from the far PBs is more likely to decrease, which may reduce the sensor active probability in AD-WPT.

As ρ increases from 0 to ∞, the number of beams of most PBs decreases from N to 1, and then increases from 1, 2, $\cdots$, to N. With fewer beams, the increased power intensity of the near PBs and decreased power opportunity of the far PBs have positive and negative impacts on the sensor active probability F_s, respectively. Whether the near PBs or the far PBs dominate F_s depends on the PB power/density and radius ρ. If the PB power/density is low or ρ is large, the near PBs dominate F_s due to the severe power attenuation of the far PBs, and vice versa.

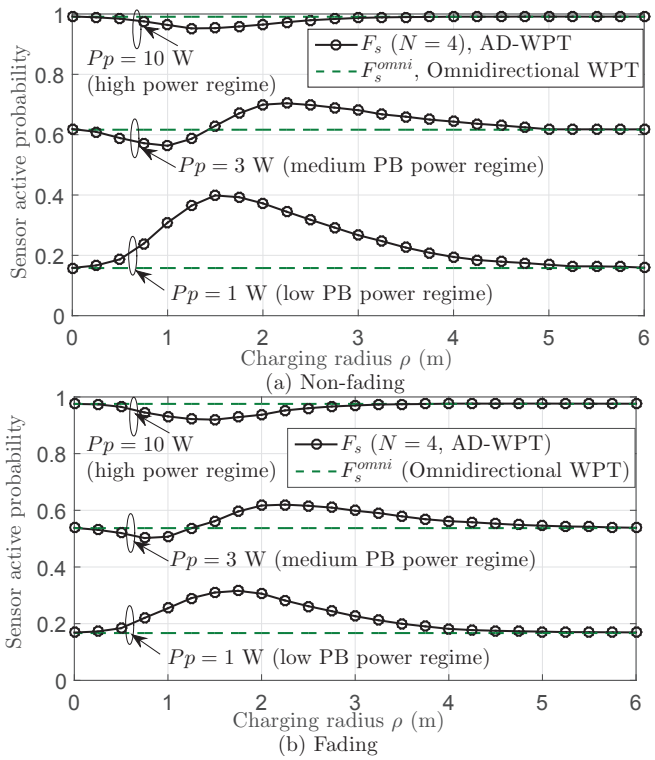

Fig. 3. Sensor active probability versus charging radius with various PB power for non-fading case and fading case ($\lambda_p = 0.1$ nodes/m^2, $\lambda_s = 0.2$ nodes/m^2, $P_s^{th} = 0.1$ mW, $\nu = 0.1$ m and $\alpha = 3$).

B. Optimal Charging Radius for Active Probability Maximization

In the following, we analyze the optimal charging radius ρ^* that maximizes the sensor active probability F_s at the typical SN_0, i.e.,

$$\text{P2}: \quad F_s^* = \max_{0<\rho<\infty} \quad F_s. \tag{36}$$

In Fig. 3 (a), we show the simulation results of the sensor active probabilities F_s in AD-WPT and F_s^{omni} in omnidirectional WPT against ρ with various P_p for non-fading case. It can be proved that the sensor active probability F_s increases with the increased PB power P_p and/or PB density λ_p. We discuss F_s by considering different power regimes of the PBs.
Case 1: Low PB power/density regime. When the PBs have low power P_p and/or density λ_p, e.g., $P_p = 1$ W in Fig. 3 (a), the near PBs dominate F_s and we have $F_s > F_s^{omni}$. F_s increases and then decreases with ρ mainly due to the decreased and increased power intensity of the PBs, respectively. There exists an optimal ρ^* (e.g., $\rho = 1.5$) that maximizes F_s.
Case 2: Medium PB power/density regime. When the PBs have medium power P_p and/or density λ_p, e.g., $P_p = 3$ W in Fig. 3 (a), the far PBs dominate F_s for small ρ with $F_s \leq F_s^{omni}$, and the near PBs dominate F_s for large ρ with

This article has been accepted for publication in a future issue of this journal, but has not been fully edited. Content may change prior to final publication. Citation information: DOI 10.1109/JSAC.2016.2551619, IEEE Journal on Selected Areas in Communications

$F_s > F_s^{omni}$, respectively. There exists an optimal ρ^* (e.g., $\rho = 2.25$) that maximizes F_s in the region of $F_s > F_s^{omni}$.

Case 3: High PB power/density regime. When the PBs have high power P_p and/or density λ_p, e.g., $P_p = 10$ W in Fig. 3 (a), we have $F_s < F_s^{omni}$. Due to the high PB power, the sensor active probability F_s^{omni} for omnidirectional WPT is high. For AD-WPT, F_s decreases and then increases with ρ mainly due to the decreased and increased power opportunity of the far PBs, respectively. As $\rho \to 0$ or $\rho \to \infty$, we have $F_s \to F_s^{omni}$ (see Corollary 1, (32) and (33)). The optimal ρ^* approaches 0 or ∞ as in omnidirectional WPT.

In Fig. 3 (b), we study the effect of fading on sensor active probability F_s. It shows that the sensor active probability for fading case is generally smaller than that for the non-fading case in Fig. 3 (a). As discussed in Section III-C, the variance of the received power under Rayleigh fading is twice as that of the non-fading case. It is highly likely that the more power fluctuation increases the probability that the received power P_s drops below the threshold P_s^{th}, which reduces the sensor active probability. We also notice an exception. In the low power regime of $P_p = 1$ W, the sensor active probability F_s^{omni} for fading case is a slightly higher than its non-fading counterpart. In this case, the sensor active probability is low and the power fluctuation increases the small chance that the received power is beyond the threshold.

From the above discussions, we see that the maximum sensor active probability in AD-WPT with the optimal charging radius ρ^* is larger than or at least equivalent to that in omnidirectional WPT, where the optimal ρ^* can be obtained via one-dimensional search.

VI. Numerical Results

In this section, we present the simulation results of the maximum average received power for flexible-task WSN and the maximum sensor active probability for equal-task WSN under the proposed AD-WPT scheme, respectively. The performance of omnidirectional WPT scheme is used as a comparison benchmark. Throughout this section, we set the wavelength value as $\nu = 0.1$ m (wavelength for microwave is between 1 mm and 1 m), and reference distance as $d_0 = 1$ m. The corresponding value of σ given in Footnote 7 is $\sigma = -41.9842$ dB [27]. We set the sensor operational power threshold to be $P_s^{th} = 0.1$ mW (power consumption for low-power devices may vary from μW to mW). Assuming Rayleigh fading, the channel power gain h_{X_i} follows i.i.d. exponential distribution with unit mean.

A. Maximum Average Received Power for Flexible-task WSN

Fig. 4 shows that both the maximum average received power $\mathbb{E}[P_s]^*$ and the corresponding optimal charging radius ρ^* increase with the increased number of PB sectors N. As N increases, the PBs are able to form narrower energy beams with higher power intensity towards the intended SNs. As a result, the coverage of PBs in AD-WPT extends and it is more beneficial to use a larger charging radius ρ^* as shown in Fig. 4 (a) to serve more SNs efficiently. With the decreased

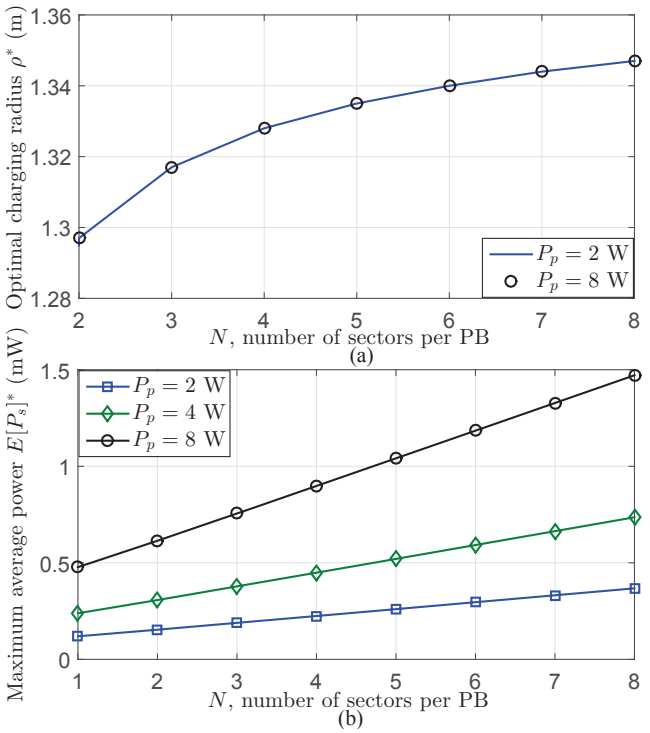

Fig. 4. (a) Optimal charging radius ρ^* for average power maximization versus N ($\lambda_p = 0.1$ nodes/m^2, $\lambda_s = 0.2$ nodes/m^2 and $\alpha = 3$). (b) Maximum average received power $\mathbb{E}[P_s]^*$ versus N ($\lambda_p = 0.1$ nodes/m^2, $\lambda_s = 0.2$ nodes/m^2 and $\alpha = 3$).

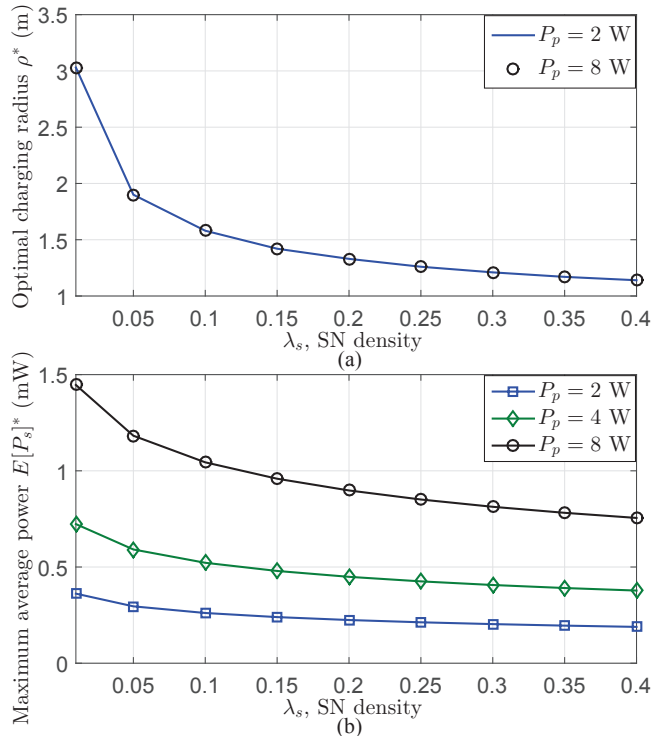

Fig. 5. (a) Optimal charging radius ρ^* for average power maximization versus λ_s ($\lambda_p = 0.1$ nodes/m^2, $\alpha = 3$ and $N = 4$). (b) Maximum average received power $\mathbb{E}[P_s]^*$ versus λ_s ($\lambda_p = 0.1$ nodes/m^2, $\alpha = 3$ and $N = 4$).

This article has been accepted for publication in a future issue of this journal, but has not been fully edited. Content may change prior to final publication. Citation information: DOI 10.1109/JSAC.2016.2551619, IEEE Journal on Selected Areas in Communications

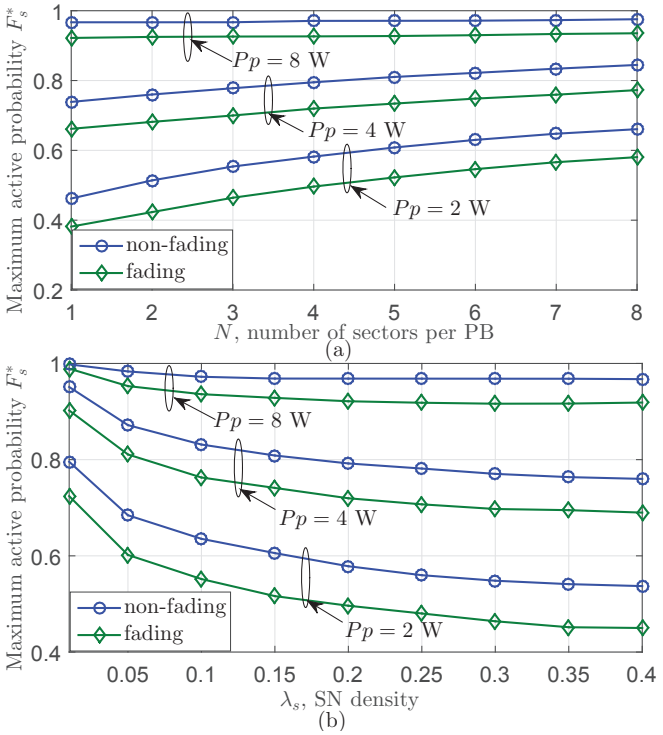

Fig. 6. Maximum sensor active probability F_s^*. (a) F_s^* versus N ($\lambda_p = 0.1$ nodes/m^2, $\lambda_s = 0.2$ nodes/m^2, $P_s^{th} = 0.1$ mW and $\alpha = 3$). (b) F_s^* versus λ_s nodes/m^2 ($\lambda_p = 0.1$ nodes/m^2, $N = 4$, $P_s^{th} = 0.1$ mW and $\alpha = 3$).

beamwidth, the power intensity of the near PBs increases, which thus improves $\mathbb{E}[P_s]^*$ as shown in Fig. 4 (b).

Fig. 5 illustrates that the maximum average received power $\mathbb{E}[P_s]^*$ and the corresponding optimal charging radius ρ^* decrease with the increased SN density λ_s. As λ_s increases, more sectors of PBs are activated. The PBs form more energy beams with lower power intensity towards the intended SNs. As a result, the PBs shrink the charging radius in AD-WPT as shown in Fig. 5 (a) to serve fewer SNs efficiently. In Fig. 5 (b), $\mathbb{E}[P_s]^*$ decreases with the increased λ_s due to the decreased power intensity of the near PBs.

In Fig. 4 and Fig. 5, we observe that $\mathbb{E}[P_s]^*$ increases linearly with the increased PB power P_p. Note ρ^* is regardless of P_p because the stationary point of $\mathbb{E}[P_s]$ is independent of P_p based on (46) and (47). It can also be deduced that increasing λ_p has a similar impact on $\mathbb{E}[P_s]^*$ as increasing P_p. Moreover, when P_p is relatively high (e.g., $P_p = 8$ W), increasing N or decreasing λ_s leads to more significant improvement of $\mathbb{E}[P_s]^*$ as shown in Fig. 4 (b) and Fig. 5 (b), respectively.

B. Maximum Sensor Active Probability for Equal-task WSN

In Fig. 6 (a), the maximum sensor active probability F_s^* increases with the increased N. As discussed in Section V, the improvement of the sensor active probability in AD-WPT compared with omnidirectional WPT is mainly due to the higher power intensity of the near PBs. As N increases, the beamwidth of the PBs decreases, which improves the power intensity and thus improves F_s^*. Fig. 6 (b) shows that the maximum sensor active probability F_s^* decreases with the increased λ_s. As λ_s increases, the near PBs are likely to form more beams with lower power intensity, which therefore reduces F_s^*. Furthermore, we notice that increasing N or decreasing λ_s results in more significant improvement of F_s^* for relative small P_p (e.g., $P_p = 2$ W). The improvement is less significant for relatively large PB power (e.g., $P_p = 8$ W) since the sensor active probability in omnidirectional WPT is already high and may not be much improved by AD-WPT. Furthermore, the maximum sensor active probability for fading case is lower than that without fading. In Rayleigh fading, as we discussed, the average received power is the same but the variance is twice as much as that without fading. Due to the channel fluctuation, the received power is more likely to drop below the target threshold, which reduces the sensor active probability.

C. Comparison with Other Power Allocation Schemes

For the AD-WPT scheme in Section II-A, we adopt uniform power allocation for the PBs, i.e., uniformly allocating the PB power among all active sectors that have at least one SN. If the exact number of SNs in each sector is known, the PBs may adopt unequal power allocation schemes which allocate the PB power according to the number of SNs in each sector. In this subsection, we mainly discuss two other power allocation schemes: greedy scheme and robust scheme. In greedy scheme, each PB allocates all power to the sector that has the largest number of SNs and no power to all other sectors. It can be easily shown that this scheme provides the maximum sum received power of all SNs in the charging region of a PB. In robust scheme, each PB allocates power proportionally to the number of SNs in each sector.

In Fig. 7 (a) and Fig. 7 (b), we compare the maximum average received power and the maximum sensor active probability for the three power allocation schemes in non-fading case, respectively. Fig. 7 (a) shows that the maximum average received power for the three schemes is similar with very minor gaps. Greedy scheme performs the best and robust scheme slightly outperforms uniform scheme in terms of average received power. In Fig. 7 (b), we see that the maximum sensor active probability of robust scheme is the highest, which slightly outperforms that of uniform scheme. The sensor active probability of greedy scheme is the lowest.

To sum up, greedy scheme shows the highest average received power but at the cost of lowest sensor active probability. It is because the single narrow-beam strategy in greedy scheme improves the power intensity but also reduces the power opportunity towards SN_0. Moreover, robust scheme outperforms uniform scheme in both average power and active probability of the SNs, but the improvement is insignificant. For greedy and robust schemes, the exact number of SNs in each sector is required and the derivation of the distribution of the received power in a heterogeneous network is more complicated than uniform scheme since the gain of the PB becomes a continuous instead of discrete variable. For uniform scheme, each PB needs only the information of the existence of SNs in each sector. It provides acceptable average power and active probability with less implementation complexity.

This article has been accepted for publication in a future issue of this journal, but has not been fully edited. Content may change prior to final publication. Citation information: DOI 10.1109/JSAC.2016.2551619, IEEE Journal on Selected Areas in Communications

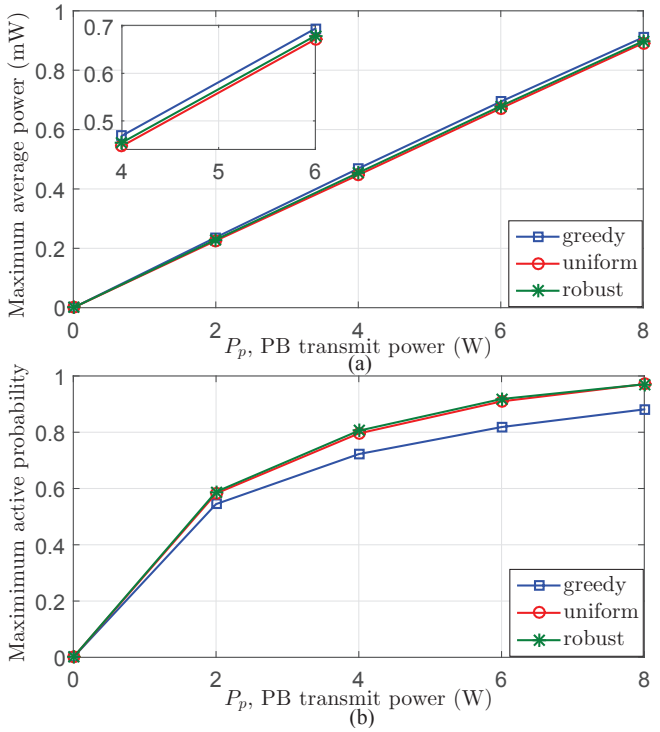

Fig. 7. Comparison of three power allocation schemes in non-fading case ($\lambda_p = 0.1$ nodes/m^2, $\lambda_s = 0.2$ nodes/m^2, $P_s^{th} = 0.1$ mW, $N = 4$ and $\alpha = 3$). (a) maximum average received power; (b) maximum sensor active probability.

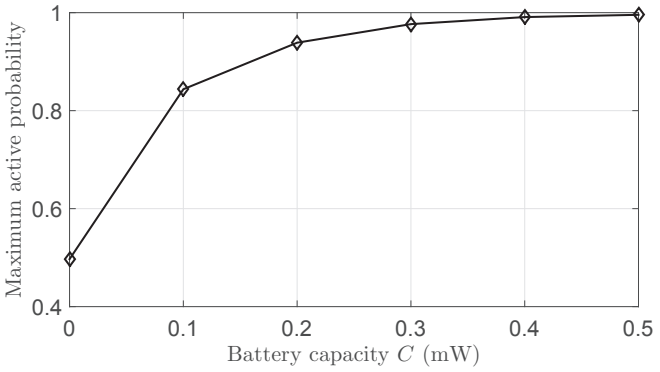

Fig. 8. Sensor active probability versus battery capacity C ($N = 4$, $P_p = 2$ W, $\lambda_p = 0.1$ nodes/m^2, $\lambda_s = 0.2$ nodes/m^2, $P_s^{th} = 0.1$ mW, $\nu = 0.1$ m and $\alpha = 3$).

D. Finite Battery Capacity

For some WSNs with relatively large-size sensors, rechargeable battery storage modules can be installed, which enables the SNs to carry forward the excessive received power for future usage (see, e.g., [30]). As the received power is used up at all sensors in flexible-task scenario, we look at the equal-task scenario, where the sensor active probability depends on the remaining energy in the battery. We consider 10^4 time frames, where each time frame consists of energy harvesting slot and energy consumption slot (for simplicity, both have the duration of 1 s). If the remaining energy at the end of energy harvesting slot is beyond the threshold P_s^{th}, the SN uses power P_s^{th} in energy consumption slot for sensing/data transmission. If there is any leftover energy after energy consumption, the SN stores at most power C in the battery and carries it forward to the next time frame. In Fig. 8, it is shown that the maximum sensor active probability increases with the increased battery capacity C. Intuitively, with larger C, an SN can store more unused power for the next frame, which increases the next-frame's power supply and thus increases the sensor active probability.

VII. Conclusions

In this paper, we proposed an AD-WPT scheme in a large-scale sensor network, where the PBs charge the SNs by adapting the energy beamforming strategies to the nearby SN locations. By using stochastic geometry, we derived the distribution metrics of the aggregate received power at a typical SN. For flexible-task and equal-task WSN, the optimal radii in AD-WPT were designed to maximize the average received power and maximize the sensor active probability, respectively. The results show that the maximum average received power and maximum sensor active probability increase with the increased density and power of the PBs, while they decrease with the increased density of the SNs and energy beamwidth. Moreover, the optimal AD-WPT is more energy efficient than omnidirectional WPT by achieving equivalent average received power or sensor active probability with less transmit power consumptions. In the future work, more practical fading scenarios such as Rician fading can be considered to address the possible line-of-sight components for short range WPT.

Appendix

A. Proof of Lemma 3

Taking the Laplace transform of (17), we have

$$\begin{aligned}
\mathcal{L}_{P_{s,n}^M}(s) &= \mathbb{E}\left[\exp\left(-sP_{s,n}^M\right)\right] \\
&= \mathbb{E}\left[\exp\left[-sP_p\sigma \sum_{X_i\in\Phi_{p,n}^M} h_{X_i} G_M \left[\max\left(\|X_i\|,1\right)\right]^{-\alpha}\right]\right] \\
&\overset{(a)}{=} \mathbb{E}\left[\prod_{X_i\in\Phi_{p,n}^M} \mathbb{E}_{h_{X_i}}\left[\exp\left[-sP_p\sigma h_{X_i} G_M \right.\right.\right. \\
&\quad \left.\left.\left. \times \left[\max\left(\|X_i\|,1\right)\right]^{-\alpha}\right]\right]\right] \\
&\overset{(b)}{=} \exp\left[-\lambda_p\beta_{M,n}\int_0^{2\pi}\int_0^{\rho}\left[1-\mathbb{E}_{h_{X_i}}\left[\exp\left[-sP_p\sigma h_{X_i} G_M \right.\right.\right.\right. \\
&\quad \left.\left.\left.\left. \times \left[\max\left(r,1\right)\right]^{-\alpha}\right]\right] r d\psi dr\right]\right] \\
&= \exp\left[-\lambda_p\beta_{M,n}\mathbb{E}_{h_{X_i}}\left[\int_0^{2\pi}\int_0^{\rho}\left[1-\exp\left[-sP_p\sigma h_{X_i} G_M \right.\right.\right.\right. \\
&\quad \left.\left.\left.\left. \times \left[\max\left(r,1\right)\right]^{-\alpha}\right]\right] r d\psi dr\right]\right], \qquad (37)
\end{aligned}$$

This article has been accepted for publication in a future issue of this journal, but has not been fully edited. Content may change prior to final publication. Citation information: DOI 10.1109/JSAC.2016.2551619, IEEE Journal on Selected Areas in Communications

where r and ψ denote the radial coordinate and angular coordinate in polar coordinate system. The step (a) follows from channel independence and step (b) is obtained by applying probability generating functional (PGFL) [7, A.3]. For $0<\rho\leq 1$, (37) is further derived as

$$\mathcal{L}_{P^M_{s,n}}(s)=\exp\Bigg[-2\pi\lambda_p\beta_{M,n}\times\mathbb{E}_{h_{X_i}}\left[\int_0^{\rho}\left[1-\exp\left(-sP_p\sigma h_{X_i}G_M\right)\right]rdr\right]\Bigg]. \quad (38)$$

For $1<\rho<\infty$, (37) is further derived as

$$\mathcal{L}_{P^M_{s,n}}(s)=\exp\Bigg[-2\pi\lambda_p\beta_{M,n}\mathbb{E}_{h_{X_i}}\left[\int_0^{1}\left[1-\exp\left(-sP_p\sigma h_{X_i}G_M\right)\right]rdr+\int_1^{\rho}\left[1-\exp\left(-sP_p\sigma h_{X_i}G_Mr^{-\alpha}\right)\right]rdr\right]\Bigg]. \quad (39)$$

From (38) and (39), we can easily obtain Lemma 3.

B. Proof of Corollary 1

As $\rho\to 0$, it holds that $M=0$ for all PBs. According to (1), we have $G_0=1$. Since $\lim_{\rho\to 0}p=1$, we have $\beta_{M,f}=1$ in Lemma 2. From Lemma 3 and Lemma 4, we have

$$\lim_{\rho\to 0}\mathcal{L}_{P^0_{s,n}(1)}(s)=1 \quad (40)$$

and

$$\lim_{\rho\to 0}\mathcal{L}_{P^0_{s,f}(1)}(s)=\exp\Bigg[-\lambda_p\pi\mathbb{E}_{h_{X_i}}\left[\left(sP_p\sigma h_{X_i}\right)^{\frac{2}{\alpha}}\times\gamma\left(1-\frac{2}{\alpha},sP_p\sigma h_{X_i}\right)\right]\Bigg]. \quad (41)$$

Substituting $M=0$, (40) and (41) into Proposition 1, we have $\lim_{\rho\to 0}\mathcal{L}_{P_s}(s)=\mathcal{L}_{P_s^{omni}}(s)$.

As $\rho\to\infty$, it holds that $M=N$ for all PBs. According to (2), we have $G_N=1$. Since $\lim_{\rho\to\infty}p=0$, we have $\beta_{M,n}=1$ in Lemma 1. From Lemma 3 and Lemma 4, we have

$$\lim_{\rho\to\infty}\mathcal{L}_{P^N_{s,n}(2)}(s)=\exp\Bigg[-\lambda_p\pi\mathbb{E}_{h_{X_i}}\left[\left(sP_p\sigma h_{X_i}\right)^{\frac{2}{\alpha}}\times\gamma\left(1-\frac{2}{\alpha},sP_p\sigma h_{X_i}\right)\right]\Bigg] \quad (42)$$

and

$$\lim_{\rho\to\infty}\mathcal{L}_{P^N_{s,f}(2)}(s)=1. \quad (43)$$

Substituting $M=N$, (42) and (43) into Proposition 1, we have $\lim_{\rho\to\infty}\mathcal{L}_{P_s}(s)=\mathcal{L}_{P_s^{omni}}(s)$.

C. Proof of Proposition 2

In this appendix, we derive $\mathbb{E}[P_s]$ in Proposition 2 by considering the following two cases.

1) $0<\rho\leq 1$*:* Taking the first derivative of the Laplace transform in Proposition 1 for $0<\rho\leq 1$, we have

$$\begin{aligned}\mathbb{E}[P_s]|_{0<\rho\leq 1}&=-\frac{d}{ds}\Big[\log\left(\mathcal{L}_{P_s}(s)|_{0<\rho\leq 1}\right)\Big]\Big|_{s=0}\\&=-\lambda_p\pi\rho^2\sum_{M=1}^{N}\beta_{M,n}\frac{d}{ds}\Big[\mathbb{E}_{h_{X_i}}\big[\exp\left(-sP_p\sigma G_Mh_{X_i}\right)\big]\Big]\Big|_{s=0}\\&\quad+\lambda_p\pi\rho^2\sum_{M=0}^{N}\beta_{M,f}\frac{d}{ds}\Big[\mathbb{E}_{h_{X_i}}\big[\exp\left(-sP_p\sigma G_Mh_{X_i}\right)\big]\Big]\Big|_{s=0}\\&\quad+\lambda_p\pi\sum_{M=0}^{N}\beta_{M,f}\frac{d}{ds}\Bigg[\mathbb{E}_{h_{X_i}}\Bigg[\left(sP_p\sigma G_Mh_{X_i}\right)^{\frac{2}{\alpha}}\times\gamma\left(1-\frac{2}{\alpha},sP_p\sigma G_Mh_{X_i}\right)\Bigg]\Bigg]\Big|_{s=0}.\end{aligned} \quad (44)$$

By further derivation, we have

$$\begin{aligned}&\frac{d}{ds}\Big[\mathbb{E}_{h_{X_i}}\big[\exp\left(-sP_p\sigma G_Mh_{X_i}\right)\big]\Big]\Big|_{s=0}\\&=\mathbb{E}_{h_{X_i}}\Big[\frac{d}{ds}\big[\exp\left(-sP_p\sigma G_Mh_{X_i}\right)\big]\Big]\Big|_{s=0}\\&=\mathbb{E}_{h_{X_i}}\Big[-P_p\sigma G_Mh_{X_i}\exp\left(-sP_p\sigma G_Mh_{X_i}\right)\Big]\Big|_{s=0}\\&=-P_p\sigma G_M\mathbb{E}\left[h_{X_i}\right]\end{aligned} \quad (45)$$

and

$$\lim_{s\to 0}\frac{d}{ds}\Bigg[\mathbb{E}_{h_{X_i}}\left[\left(P_p\sigma G_Mh_{X_i}s\right)^{\frac{2}{\alpha}}\gamma\left(1-\frac{2}{\alpha},P_p\sigma G_Mh_{X_i}s\right)\right]\Bigg]=\frac{P_p\sigma G_M\alpha\mathbb{E}\left[h_{X_i}\right]}{\alpha-2}. \quad (46)$$

Substituting (45) and (46) into (44) yields

$$\mathbb{E}[P_s]|_{0<\rho\leq 1}=P_p\lambda_p\pi\sigma\mathbb{E}\left[h_{X_i}\right]\left[\rho^2\left(\sum_{M=1}^{N}\beta_{M,n}G_M-\sum_{M=0}^{N}\beta_{M,f}G_M\right)+\frac{\alpha}{\alpha-2}\sum_{M=0}^{N}\beta_{M,f}G_M\right]. \quad (47)$$

We further obtain

$$\sum_{M=1}^{N}\beta_{M,n}G_M=\frac{1-p^N}{1-p} \quad (48)$$

and

$$\sum_{M=0}^{N}\beta_{M,f}G_M=(p+q)^M=1. \quad (49)$$

Substituting (48) and (49) back into (47), we obtain (25a) in Proposition 2.

2) $1<\rho<\infty$*:* Taking the first derivative of the Laplace transform in Proposition 1 for $1<\rho<\infty$, we have

$$\begin{aligned}\mathbb{E}[P_s]|_{1<\rho<\infty}&=-\frac{d}{ds}\Big[\log\left(\mathcal{L}_{P_s}(s)|_{1<\rho<\infty}\right)\Big]\Big|_{s=0}\\&=P_p\lambda_p\pi\sigma\mathbb{E}\left[h_{X_i}\right]\left[\frac{\alpha}{\alpha-2}\sum_{M=1}^{N}\beta_{M,n}G_M+\frac{2\rho^{2-\alpha}}{\alpha-2}\times\left(\sum_{M=0}^{N}\beta_{M,f}G_M-\sum_{M=1}^{N}\beta_{M,n}G_M\right)\right].\end{aligned} \quad (50)$$

Substituting (48) and (49) into (50), we obtain (25b) in Proposition 2.

This article has been accepted for publication in a future issue of this journal, but has not been fully edited. Content may change prior to final publication. Citation information: DOI 10.1109/JSAC.2016.2551619, IEEE Journal on Selected Areas in Communications

D. Proof of Corollary 2

We compare (26) with (25a) and (25b), respectively. Firstly, (25a) is compared with (26).

$$\mathbb{E}\left[P_s\right]|_{0<\rho\leq 1} - \mathbb{E}\left[P_s^{omni}\right] = P_p\lambda_p\pi\sigma\rho^2\mathbb{E}\left[h_{X_i}\right]\frac{p-p^N}{1-p},$$

where p is given in (6). For $\rho \to 0$, we have $p \to 1$ and $\mathbb{E}\left[P_s\right]|_{0<\rho\leq 1} \to \mathbb{E}\left[P_s^{omni}\right]$. For $0 < \rho \leq 1$, we have $p^N < p < 1$, which leads to $\mathbb{E}\left[P_s\right]|_{0<\rho\leq 1} > \mathbb{E}\left[P_s^{omni}\right]$.

Secondly, (25b) is compared with (26) as follows.

$$\begin{aligned}&\mathbb{E}\left[P_s\right]|_{1<\rho<\infty} - \mathbb{E}\left(P_s^{omni}\right)\\ &= P_p\lambda_p\pi\sigma\mathbb{E}\left[h_{X_i}\right]\frac{\alpha-2\rho^{2-\alpha}}{\alpha-2}\frac{p-p^N}{1-p}.\end{aligned} \tag{51}$$

For $\rho \to \infty$, we have $p \to 0$ and $\mathbb{E}\left[P_s\right]|_{1<\rho<\infty} \to \mathbb{E}\left[P_s^{omni}\right]$. For $1 < \rho < \infty$, we have $p^N < p < 1$. Since $\alpha > 2$, we further have $\rho^{2-\alpha} < 1$ and $\alpha > 2\rho^{2-\alpha}$. Then, it is proved that $\mathbb{E}\left[P_s\right]|_{1<\rho<\infty} > \mathbb{E}\left[P_s^{omni}\right]$.

E. Proof of Proposition 3

Taking the second derivative of the Laplace transform in Proposition 1, we have

$$\begin{aligned}\mathbb{V}[P_s]|_{0<\rho\leq 1} &= \frac{d^2}{ds^2}\left[\log\left(\mathcal{L}_{P_s}(s)|_{0<\rho\leq 1}\right)\right]\Big|_{s=0}\\ &= \lambda_p\pi\rho^2\sum_{M=1}^{N}\beta_{M,n}\frac{d^2}{ds^2}\left[\mathbb{E}_{h_{X_i}}\left[\exp\left(-sP_p\sigma G_M h_{X_i}\right)\right]\right]\Big|_{s=0}\\ &\quad - \lambda_p\pi\rho^2\sum_{M=0}^{N}\beta_{M,f}\frac{d^2}{ds^2}\left[\mathbb{E}_{h_{X_i}}\left[\exp\left(-sP_p\sigma G_M h_{X_i}\right)\right]\right]\Big|_{s=0}\\ &\quad - \lambda_p\pi\sum_{M=0}^{N}\beta_{M,f}\frac{d^2}{ds^2}\left[\mathbb{E}_{h_{X_i}}\left[\left(sP_p\sigma G_M h_{X_i}\right)^{\frac{2}{\alpha}}\right.\right.\\ &\quad \left.\left.\times\,\gamma\left(1-\frac{2}{\alpha}, sP_p\sigma G_M h_{X_i}\right)\right]\right]\Big|_{s=0}.\end{aligned} \tag{52}$$

By further derivation, we have

$$\begin{aligned}&\frac{d^2}{ds^2}\left[\mathbb{E}_{h_{X_i}}\left[\exp\left(-sP_p\sigma G_M h_{X_i}\right)\right]\right]\Big|_{s=0}\\ &= \left(P_p\sigma G_M\right)^2\mathbb{E}\left[\left(h_{X_i}\right)^2\right]\end{aligned} \tag{53}$$

and

$$\begin{aligned}&\lim_{s\to 0}\frac{d^2}{ds^2}\left[\mathbb{E}_{h_{X_i}}\left[\left(sP_p\sigma G_M h_{X_i}\right)^{\frac{2}{\alpha}}\right.\right.\\ &\qquad\left.\left.\times\,\gamma\left(1-\frac{2}{\alpha}, sP_p\sigma G_M h_{X_i}\right)\right]\right]\\ &= -\frac{\alpha}{\alpha-1}\left(P_p\sigma G_M\right)^2\mathbb{E}\left[\left(h_{X_i}\right)^2\right].\end{aligned} \tag{54}$$

Substituting (53) and (54) into (52) yields (30a). Similarly, we can obtain $\mathbb{V}[P_s]|_{1<\rho<\infty}$ in (30b).

REFERENCES

[1] I. Akyildiz, W. Su, Y. Sankarasubramaniam, and E. Cayicrci, "A survey on sensor networks," *IEEE Commun. Mag.*, vol. 40, no. 8, pp. 102-114, Aug. 2002.

[2] S. Bi, C. K. Ho, and R. Zhang, "Wireless powered communication: opportunities and challenges," *IEEE Commun. Mag.*, vol. 53, no. 4, pp. 117-125, Apr. 2015.

[3] X. Lu, P. Wang, D. Niyato, D. I. Kim, and Z. Han, "Wireless networks with RF energy harvesting: A contemporary survey," *IEEE Commun. Surveys Tuts.*, vol. 17, no. 2, pp. 757-789, Second Quarter 2015.

[4] M. Erol-Kantarci and H. T. Mouftah,, "Suresense: sustainable wireless rechargeable sensor networks for the smart grid," *IEEE Wireless Commun.*, vol. 19, no. 3, pp. 30-36, Jun. 2012.

[5] L. Xie, Y. Shi, Y. T. Hou, and W. Lou, "Wireless power transfer and applications to sensor networks," *IEEE Wireless Commun.*, vol. 20, no. 4, pp. 140-145, Aug. 2013.

[6] Z. Popovic, E. A. Falkenstein, D. Costinett, and R. Zane, "Low-power far-field wireless powering for wireless sensors," *Proc. IEEE*, vol. 101, no. 6, pp. 1397-1409, Jun. 2013.

[7] M. Haenggi and R. K. Ganti, *Interference in Large Wireless Networks,* Now Publishers, 2008.

[8] M. Heanggi, J. G. Andrews, F. Baccelli, O. Dousse, and M. Franceschetti, "Stochastic geometry and random graphs for analysis and design of wireless networks," *IEEE J. Sel. Areas Commun.*, vol. 27, no. 7, pp. 1029-1046, Sep. 2009.

[9] J. G. Andrews, F. Baccelli, and R. K. Ganti, "A tractable approach to coverage and rate in cellular networks," *IEEE Trans. Commun.*, vol. 59, no. 11, pp. 3122-3134, Nov. 2011.

[10] H. ElSawy, E. Hossain, and M. Heaggi, "Stochastic geometry for modeling, analysis, and design of multi-tier and cognitive cellular wireless networks: A survey," *IEEE Commun. Surveys Tuts.*, vol. 15, no. 3, pp. 996-1019, Third Quarter, 2013.

[11] X. Zhou, R. Zhang, and C. K. Ho, "Wireless information and power transfer: architecture design and rate-energy tradeoff," *IEEE Trans. Commun.,* vol. 61, no. 11, pp. 4757-4767, Nov. 2013.

[12] H. Ju and R. Zhang, "Throughput maximization in wireless powered communication networks," *IEEE Trans. Wireless Commun.,* vol. 13, no. 1, pp. 418-428, Jan. 2014.

[13] S. H. Lee, R. Zhang, and K. B. Huang, "Opportunistic wireless energy harvesting in cognitive radio networks," *IEEE Trans. Wireless Commun.,* vol. 12, no. 9, pp. 4788-4799, Sep. 2013.

[14] Y. L. Che, L. Duan, and R. Zhang, "Spatial throughput maximization in large scale wireless powered communication networks," *IEEE J. Sel. Areas Commun.,* vol. 33, no. 8, pp. 1534-1548, Aug. 2015.

[15] A. A. Nasir, X. Zhou, S. Durrani, and R. A. Kennedy, "Relaying protocols for wireless energy harvesting and information processing," *IEEE Trans. Wireless Commun.,* vol. 12, no. 7, pp. 3622-3636, Jul. 2013.

[16] D. S. Michalopoulos, H. A. Suraweera, and R. Schober, "Relay selection for simultaneous information transmission and wireless energy transfer: A tradeoff perspective," *IEEE J. Sel. Areas Commun.*, vol. 33, no. 8, pp. 1578-1594, Aug. 2015.

[17] I. Krikidis, "Simultaneous information and energy transfer in large-scale networks with/without relaying," *IEEE Trans. Commun.*, pp. 900-912, vol. 62, no. 3, Mar. 2014.

[18] H. Ju and R. Zhang, "User cooperation in wireless powered communication networks," in *Proc. IEEE Global Commun. Conf. (GLOBECOM 2014)*, pp. 1430 - 1435, Austin, TX, Dec. 8-12, 2014.

[19] S. Gong, L. Duan, and N. Gautam, "Optimal scheduling and beamforming design in relay networks with energy harvesting constraints," *IEEE Trans. Wireless Commun.,* vol. 15, no. 2, pp. 1226-1238, Feb. 2016.

[20] J. Xu and R. Zhang, "Energy beamforming with one-bit feedback," *IEEE Trans. Signal Process.,* vol. 62, no. 20, pp. 5370-5381, Oct. 2014.

[21] R. Zhang and C. K. Ho, "MIMO broadcasting for simultaneous wireless information and power transfer," *IEEE Trans. Wireless Commun.,* vol. 12 , no. 5, pp. 1989-2001, May 2013.

[22] J. Xu, L. Liu, and R. Zhang, "Multiuser MISO beamforming for simultaneous wireless information and power transfer," *IEEE Trans. Signal Process.,* vol. 62, no. 18, pp. 4798-4810, Sep. 2014.

[23] K. Huang and V. K. N. Lau, "Enabling wireless power transfer in cellular networks: Architecture, modeling and deployment," *IEEE Trans. Wireless Commun.*, vol. 13, no. 2, pp. 902-912, Feb. 2014.

[24] J. Xu, L. Duan, and R. Zhang, "Energy group-buying with loading sharing for green cellular networks," *IEEE J. Sel. Areas Commun.,* forthcoming. [Online]. http://arxiv.org/abs/1508.06093

[25] S. Cai, Y. Che, L. Duan, J. Wang, S. Zhou, and R. Zhang, "Green heterogeneous networks through dynamic small-cell operation," *IEEE J. Sel. Areas Commun.,* forthcoming. [Online]. http://arxiv.org/pdf/1601.01453v1.pdf

[26] C. A. Balanis, *Antenna Theory: Analysis and Design (Third Edition),* Wiley, 2005.

[27] A. Goldsmith, *Wireless Communications,* Cambridge. University Press, 2005.

[28] J. J. Shynk, *Probability, Random Variables, and Random Processes: Theory and Signal Processing Applications*, Wiley, 2012.

[29] W. Liu, X. Zhou, S. Durrani, H. Mehrpouyan, and S. D. Blostein, "Performance of wireless-powered sensor transmission considering energy cost of sensing," in *Proc. IEEE Global Commun. Conf. (GLOBECOM 2015),* San Diego, CA, USA, Dec. 6-10, 2015.

[30] K. Huang, "Spatial throughput of mobile ad hoc networks powered by energy harvesting," *IEEE Trans. Inf. Theory*, vol. 59, no. 11, pp. 7597-7612, Nov. 2013.

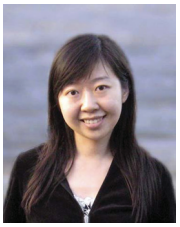

Zhe Wang (S'10-M'14) received the M.Eng.Sc degree in telecommunications engineering in 2010, and the Ph.D. degree in electrical engineering in 2014, both from The University of New South Wales, Sydney, Australia. She was a Visiting Scholar at The Hong Kong University of Science and Technology in 2011. During 2014-2015, she was as a Research Fellow with the Engineering Systems and Design Pillar, Singapore University of Technology and Design, Singapore. She is currently a Research Fellow with the Department of Electrical and Electronic Engineering, The University of Melbourne, Australia. Her research interests include cognitive radio, wireless information and power transfer, cooperative communications, and stochastic-geometric analysis for ad-hoc networks.

Lingjie Duan (S'09-M'12) received the bachelor of engineering degree from Harbin Institute of Technology, Harbin, China, in 2008, and the Ph.D. degree from the Chinese University of Hong Kong, Hong Kong, in 2012. He is an Assistant Professor with Engineering Systems and Design, Singapore University of Technology and Design (SUTD), Singapore. In 2011, he was a Visiting Scholar at the Department of Electrical Engineering and Computer Sciences, University of California at Berkeley, Berkeley, CA, USA. He is an Editor of IEEE Communications Surveys and Tutorials, and is a SWAT member in the Editorial Board of IEEE Transactions on Vehicular Technology. His research interests include network economics and game theory, cognitive communications and cooperative networking, energy harvesting wireless communications, and network security. Recently, he served as the Program Co-Chair of the IEEE INFOCOM 2014 GCCCN Workshop, ICCS 2014 special session on Economic Theory and Communication Networks, the Wireless Communication Systems Symposium of the IEEE ICCC 2015, the GCNC Symposium of the IEEE ICNC 2016, and the IEEE INFOCOM 2016 GSNC Workshop. He also served as a technical program committee (TPC) member of many leading conferences in communications and networking (e.g., ACM MobiHoc, IEEE SECON, ICC, GLOBECOM, WCNC, and NetEcon). He was the recipient of the 10th IEEE ComSoc Asia-Pacific Outstanding Young Researcher Award in 2015, the Hong Kong Young Scientist Award (Finalist in Engineering Science track) in 2014, and the CUHK Global Scholarship for Research Excellence in 2011.

Rui Zhang (S'00-M'07-SM'15) received the B.Eng. (first-class Hons.) and M.Eng. degrees from the National University of Singapore, Singapore, and the Ph.D. degree from the Stanford University, Stanford, CA, USA, all in electrical engineering, in 2000, 2001, and 2007, respectively. From 2007 to 2010, he worked with the Institute for Infocomm Research, ASTAR, Singapore, where he now holds a Senior Research Scientist joint appointment. Since 2010, he has joined the Department of Electrical and Computer Engineering, National University of Singapore, where he is now an Associate Professor. He has authored over 200 papers. His research interests include energy-efficient and energy-harvesting-enabled wireless communications, wireless information and power transfer, multiuser MIMO, cognitive radio, UAV communications, wireless security, and optimization methods. He has served as a TPC member and organizing committee member for over 30 IEEE conferences. He has been an elected member of the IEEE Signal Processing Society SPCOM and SAM Technical Committees, and served as the Vice Chair of the IEEE ComSoc Asia-Pacific Board Technical Affairs Committee. He is an Editor for the IEEE TRANSACTIONS ON WIRELESS COMMUNICATIONS, the IEEE TRANSACTIONS ON SIGNAL PROCESSING, the IEEE JOURNAL ON SELECTED AREAS IN COMMUNICATIONS (Green Communications and Networking Series). He has been listed as a Highly Cited Researcher (also known as the World's Most Influential Scientific Minds), by Thomson Reuters. He was the co-recipient of the Best Paper Award from the IEEE PIMRC in 2005, and the IEEE Marconi Prize Paper Award in Wireless Communications in 2015. He was the recipient of the 6th IEEE Communications Society Asia-Pacific Region Best Young Researcher Award in 2011, and the Young Researcher Award of the National University of Singapore in 2015.